

Oxygen Ordering Superstructures and Structural Phase Diagram of $\text{YBa}_2\text{Cu}_3\text{O}_{6+x}$ Studied by Hard X-ray Diffraction

M. v. Zimmermann*

*Hamburger Synchrotronstrahlungslabor HASYLAB at Deutsches Elektronen-Synchrotron DESY, Notkestr. 85,
D-22603 Hamburg, Germany*

T. Frello, N. H. Andersen, J. Madsen, M. Käll, O. Schmidt

Condensed Matter Physics and Chemistry Department, Risø National Laboratory, DK-4000 Roskilde, Denmark

T. Niemöller, J. R. Schneider

*Hamburger Synchrotronstrahlungslabor HASYLAB at Deutsches Elektronen-Synchrotron DESY, Notkestr. 85,
D-22603 Hamburg, Germany*

H. F. Poulsen

Materials Research Department, Risø National Laboratory, DK-4000 Roskilde, Denmark

Th. Wolf

Forschungszentrum Karlsruhe, ITP, D-76021 Karlsruhe, Germany

R. Liang, P. Dosanjh W. N. Hardy

*Department of Physics, The University of British Columbia, Vancouver, British Columbia, V6T 1Z1 Canada
(February 28, 2022)*

High energy x-ray diffraction is used to investigate the bulk oxygen ordering properties of $\text{YBa}_2\text{Cu}_3\text{O}_{6+x}$. Superstructures of Cu-O chains aligned along the b axis and ordered with periodicity ma , along the a axis have been observed. For $x < 0.62$ the only observed superstructure is ortho-II with $m = 2$. At room temperature we find ortho-III ($m = 3$) for $0.72 \leq x \leq 0.82$, ortho-V ($m = 5$) in a mixed state with ortho-II at $x = 0.62$, and ortho-VIII ($m = 8$) at $x = 0.67$. Ortho-II is a 3D ordered structural phase, the remaining ones are essentially 2D. None of the superstructures develops long range ordering. Studies of the ortho-II ordering properties in samples prepared with $x = 0.5$ but by different methods show that finite size domains with internal thermodynamic equilibrium are formed. The crystal perfection as well as the thermal annealing history determine the domain size. The temperature dependence of the observed superstructure ordering is investigated explicitly and a structural phase diagram is presented.

I. INTRODUCTION

It is now well-established that $\text{YBa}_2\text{Cu}_3\text{O}_{6+x}$ (YBCO) is antiferromagnetic (AF) in the tetragonal structural phase for $0 < x < 0.35$, and becomes superconducting at low temperatures in the weakly distorted orthorhombic phase for $0.35 \leq x < 1$. By high temperature thermal treatment in a suitable oxygen pressure it is possible to vary the oxygen composition in a continuous way^{1,2}, that changes the electronic properties from an AF insulator via an underdoped to an optimally doped high- T_c superconductor with $T_c = 93$ K, and a slightly overdoped material for $x > 0.93$. YBCO has therefore become a major model system for basic studies of high- T_c superconductivity and it is a leading candidate for technological applications.

Structural refinement of neutron diffraction data have shown that the variable amount of oxygen resides in the CuO_x basal plane³. A strong tendency towards formation and alignment of Cu-O chains gives rise to the orthorhombic distortion below the temperature dependent transition line between the tetragonal and the orthorhombic phase. The importance of oxygen ordering for the superconducting properties has been verified directly from experimental studies where crystals are quenched from the tetragonal disordered into the orthorhombic ordered phase. Here it is found that T_c of quenched YBCO is reduced compared to the equilibrium value and increases with time when the sample is annealed at room temperature⁴⁻⁷. Equally, it has been observed that the oxygen ordering of quenched YBCO crystals increases with time⁸. The consensus is therefore that the Cu-O chain ordering in the CuO_x basal plane controls the charge transfer leading to superconductivity in the CuO_2 planes. However, in spite of the very large number of experimental and theoretical model studies there is still no finite microscopic understanding of how the charge transfer is controlled by the Cu-O chain length and superstructure ordering. Thus, it is not settled how the electronic states formed in the Cu-O chains hybridize with the electronic structure in the CuO_2 planes, give rise to the charge transfer and contribute to the anisotropy of the superconducting properties. A likely explanation is that the available structural information is not sufficiently detailed and unambiguous because the oxygen diffusion kinetics is too slow at the temperatures where the superstructures become stable. It has therefore not been established which superstructures are actually formed as function of oxygen composition x , impurity level and thermal treatment, and how they influence the electronic states.

The orthorhombic phase found below the tetragonal to orthorhombic phase transition has the basic ortho-I structure, and it is formed by Cu-O chains that align along the b axis with oxygen on the so-called O(1) site, whereas the sites on the a axis (called O(5)) are essentially empty. Ortho-I is a 3D long range ordered struc-

ture, but in commonly prepared crystals true long range order is prevented by the formation of twin-domains with domain size ranging from a few hundred Ångström to macroscopic size. Clearly, there is disorder in the ortho-I chain structure for compositions $x < 1.0$. Therefore, in thermodynamic equilibrium ordered superstructures must be formed for $T \rightarrow 0$. At $x = 0.5$ an ideal 3D ortho-II superstructure may in principle be formed inside the ortho-I twin domains with perfect Cu-O chains on every second b axis and the remaining ones are empty, *i.e.* they contain only Cu. 3D ordering with the Cu-O chains stacked on top of one another along the c axis has been observed but only with finite size ordering in all three crystallographic directions.

Electron microscopy techniques have had a leading role in establishing the superstructures of YBCO⁹⁻¹². However, the need for confirmation by bulk structural techniques is generally recognized, because electron beam heating of thin crystals may change the mobile oxygen content x and generate transient non-equilibrium surface structures. Also, it is difficult to obtain quantitative details about the finite size ordering properties and their temperature dependence by these techniques. The observed superstructures include the Cu-O chain type of ordering as ortho-II as well as more complex ordering sequences of essentially full (Cu-O) and empty (Cu) chains with periodicity ma along the a axis and corresponding superstructure reflections at modulation scattering vectors: $\vec{Q} = (nh_m \ 0 \ 0)$, where $h_m = 1/m$, and $n < m$ are integers, and the coordinates refer to the reciprocal lattice vectors. Superstructure reflections with $m = 2, 3, 4, 5$ and 8 , which we shall call ortho-II, ortho-III, ortho-IV, ortho-V and ortho-VIII, respectively, have been observed experimentally. Ideally, these superstructures may be symbolized by their sequence of full (1) Cu-O and empty (0) Cu chains. Thus, ortho-II is simply (10) with $x = 1/2$, and the ortho-III sequence is (110) with composition $x = 2/3$. Ortho-IV has an ordered sequence of (1110) and composition $x = 3/4$, and ortho-V is a sequential ordering of ortho-II and ortho-III, *i.e.* (10110), with composition $x = 3/5$. Ortho-VIII is ortho-V combined with ortho-III to the sequence (10110110) and ideal composition $x = 5/8$. In principle similar structures with full and empty chains interchanged may be stable, but they have not been observed experimentally.

Superstructures with unit cells $2\sqrt{2}a \times 2\sqrt{2}a \times c$ ^{10,13,14} and $\sqrt{2}a \times 2\sqrt{2}a \times c$ ¹⁵, the so-called herringbone type, have been reported. However, as we shall discuss in Section IV these superstructures are most likely not from oxygen ordering. The ortho-II and ortho-III superstructures have been verified as bulk structural phases by x-ray^{8,15-20} and neutron^{17,21-24} diffraction techniques. The first observation by x-ray diffraction was made by Fleming *et al.*¹⁶ for ortho-II and by Plakhty *et al.*²⁵ for ortho-III. Similarly, the first neutron diffraction data were presented by Zeiske *et al.*²² for ortho-II, and by Plakhty *et al.*²³ and Schleger *et al.*²⁶ for ortho-III. Anal-

ysis of structure factors obtained from a combination of neutron and x-ray diffraction data has unequivocally shown that the ortho-II and ortho-III superstructures result from oxygen ordering in Cu-O chains^{15,20,21,27–31}. However, relaxation of cations associated with the oxygen chain ordering contributes significantly to the superstructure intensities. In particular the barium displacement has a strong influence on the x-ray diffraction intensity. The displacements show only minor variation with oxygen composition^{23,28}. Also, in the ortho-II phase there was found no significant change in the displacements as function of temperature¹⁸. Compiling previous room temperature data from x-ray and neutron diffraction studies, we find that the ortho-II superstructure has been observed for oxygen compositions $0.35 \leq x \leq 0.7$ and the ortho-III superstructure for $0.7 \leq x \leq 0.77$. As we shall present below, we have observed clear indications of bulk phase ortho-V correlations for $x = 0.62$ and ortho-VIII for $x = 0.67$, but we have found no evidence for the ortho-IV superstructure. Only a few of the previous studies have been carried out above room temperature^{8,18,19,26}.

From previous neutron and hard x-ray diffraction studies it has been inferred that the finite size ordering of ortho-II results from formation of anti-phase domains inside the ortho-I twin domains below an ordering temperature of $T_{OII} = 125(5)^\circ\text{C}$ ^{8,32}. Anisotropic superstructure reflections with a Lorentzian-squared line shape were found in the ordered state⁸ as expected from Porod’s law: $S(q) \propto \frac{1}{q^{d+1}}$ for finite size ordered domains with sharp boundaries in spatial dimension d . Studies of the ordering kinetics following a quench in temperature from the ortho-I into the ortho-II phase have shown a time dependent domain growth that is algebraic at early times and logarithmic at late times. The characteristic time of the growth process is activated with an activation energy of 1.4 eV. At 70 °C it is some days and it extrapolates to several years at room temperature. On this basis it was suggested that the finite size ordering may result from pinning of the domain walls by impurities or defects, but recent computer simulations have shown that intrinsic slowing down due to the large effective activation energy for movement of long Cu-O chains may contribute as well³³.

In the present paper we report on experimental studies of the oxygen ordering in YBCO covering the oxygen compositions $0.35 \leq x \leq 0.87$ and temperatures up to 250 °C, by diffraction of high energy synchrotron radiation (~ 100 keV). Thus, our studies do not include the region at and above the optimal doping level $x \geq 0.93$ where Kaldis *et al.* have observed structural anomalies (see *e.g.* Ref. 34). The high energy x-ray diffraction technique combines the high penetration power of neutrons with the high momentum space resolution. The penetration depth of 100 keV x-rays in YBCO is of the order of 1 mm. This assures that we probe the bulk properties of the samples and are insensitive to oxygen diffusion in and

out of the surface, and studies in sample environments with varying temperatures and controlled atmospheres are easily accessible. Finally, the synchrotron intensity is so high that scattering signals down to a factor of 10^8 smaller than the fundamental Bragg peaks can be resolved, and the kinetics of the ordering can be studied with a time resolution of 1 second. From our studies we present temperature scans of the structure factors of the superstructures, determine their phase boundaries and the nature of the ordering. Firstly, we show that the superstructures including ortho-V and ortho-VIII, that Beyers *et al.*¹² have observed by electron microscopy, represent bulk structural phases. Secondly, we present extensive studies of the ortho-II superstructure ordering in crystals of different quality and thermal treatment. Finally, we use the present structural data jointly with data compiled from previous studies to establish a structural phase diagram that includes the oxygen superstructures and the tetragonal to orthorhombic (ortho-I) transition temperature, T_{T-OI} , obtained by neutron powder diffraction. We also review and compare with structural findings by other groups and discuss our results in relation to structural model studies.

The layout of the paper is as follows: In Section II we supply information about the crystal growth and oxidation of the sample (II A), details about the experimental setup (II B), and the data analysis (II C). The experimental results are presented in Section III. First we account for the results for the ortho-II superstructure formation (III A). This includes the dependence of the ortho-II correlation length on crystal quality and thermal treatment of the sample, the phase transition into the ortho-I phase, and the stability range of the composition x . Then we describe the ordering properties and the stability range of the ortho-III superstructure (III B). In Subsections III C and III D we present the properties of the ortho-V and ortho-VIII superstructure ordering, respectively, and a structural phase diagram of the oxygen ordering is presented in Section III E. In Section IV we discuss our experimental structural results in relation to other structural findings and their importance for charge transfer, and to theoretical model descriptions. A concluding summary is given in Section V.

II. EXPERIMENTAL DETAILS

A. Sample Preparation

The single crystals used to study the different superstructure phases and establish the phase diagram were grown in YSZ (yttria-stabilized zirconia) crucibles by a flux growth method³⁵ using chemicals of 99.999 % purity for Y_2O_3 and CuO, and 99.997 % for BaCO_3 . The impurity level of the crystals has been analyzed by ICP-MS (Inductively Coupled Plasma Mass Spectroscopy). The Zr content of the crystals was found to be less than 10

ppm. by weight. The major impurities were Al, Fe and Zn, the sum of which amounts to less than 0.2 % atom per unit cell. When optimally doped ($x = 0.93$) these crystals have $T_c = 93.2$ K and the width of the 10 % - 90 % diamagnetic response is $\Delta T_c = 0.3$ K.

Of the four crystals used to study the ortho-II ordering properties as function of sample purity, crystals #1, #3 and #4 were grown by the flux growth technique described in Ref. 36, and crystal #2 as described above. Crystal #1 was used to study the ortho-II ordering properties when exposed to six different annealing methods.

YSZ crucibles, and chemicals of purity better than 99.99 % and 99.9 % were used for crystals #1 and #3, respectively. Crystal #4 was grown in a SnO₂ crucible with chemicals of purity better than 99.99 %. The impurity level of crystals #1, #3 and #4 has not been determined directly, but the flux from the crucibles used to grow crystals #1 and #4 has been analyzed. Excessive amounts of Zr and Hf (up to 15000 ppm for Zr and 550 ppm for Hf) were found, but these elements are known to have a very low solubility in YBCO. Major impurity components were Al with concentrations 200 ppm and 335 ppm in the flux from crystal #1 and crystal #4, respectively, and similarly for Eu: 115 ppm and 110 ppm. The superconducting transition temperatures and the widths of the transitions have been determined in the fully oxygenated state ($x = 0.99$). They are: $T_c = 91.0$ K, $\Delta T_c < 1.0$ K for crystal #1, $T_c = 92.0$ K, $\Delta T_c = 1.5$ K for crystal #3, and $T_c = 91.5$ K, $\Delta T_c < 0.5$ K for crystal #4. The lower T_c and larger ΔT_c values of these crystals are not necessarily a consequence of bad crystal quality but rather a result of overdoping. Thus crystal #1 has $T_c = 93.5$ K and $\Delta T_c < 0.5$ K when optimally doped. For all crystals prepared by high purity chemicals (better than 99.99 %) it is likely that the impurities come from minority components of the crucible material or from the furnace walls. All the crystals are plate-like with thicknesses of $\frac{1}{2}$ to 1 mm, flat dimensions of 1.5 to 3 mm and weights ranging from 10 to 70 mg.

The oxygen composition of the crystals was changed by use of a gas-volumetric equipment^{1,2}. For reduction or oxidation the crystals are heated with a suitable amount (≈ 10 g) of YBCO buffer powder in a quartz tube connected to an external closed volume system. High purity oxygen gas (99.999 %) is supplied to the system and the pressure is controlled and monitored by use of high precision absolute pressure gauges (MKS Baratron) with accuracy and resolution better than 0.01 %. The crystals and the powder are wrapped in platinum foil to prevent reaction with the quartz tube. The closed volume system is made of ultra-high vacuum components and contained in a thermostatically controlled environment which allows for accurate determination of the oxygen pressure and oxygen uptake by the powder and the crystals. The water adsorbed in the system and the materials is removed prior to the preparation by use of a liquid nitrogen trap and heating the quartz tube to 300 °C. At this temperature there is no reduction of the crystal and the oxygen

equilibrium pressure is in any case sufficiently low that the oxygen does not condense in the trap. The desired oxygen composition x is usually established by pumping out or adding a suitable amount of oxygen gas at temperatures between 500 and 600 °C. During subsequent cooling the oxygen pressure is reduced to assure that x stays essentially constant. A final long time annealing may be performed at lower temperatures to obtain equilibrium between the powder and the single crystals and develop the oxygen ordering superstructures. For studies of the structural phase diagram a characteristic procedure to establish the superstructure is annealing at 80 °C for 10 hours and cooling by 1 °C/hour to room temperature where the crystal is stored for more than one week before the measurements.

If the starting oxygen composition of the buffer powder is known and it is assumed that the crystals are in equilibrium with the powder, the oxygen composition may be determined with an accuracy better than $\Delta x = 0.02$ by use of the ideal gas law. The resulting oxygen composition x has been compared with the known values of the oxygen equilibrium pressure determined by Schleger *et al.*², and full agreement has been established in all cases. Crystals prepared previously by the method have been examined by neutron diffraction technique and the oxygen composition x determined from crystallographic analysis of 375 unique reflections were found to be in full agreement with the values obtained from the gas-volumetry³⁷.

B. Instrument

The experiments were performed on a triple axis diffractometer at the high-energy beam line BW5 at HASYLAB in Hamburg³⁸. The diffractometer operates in horizontal Laue scattering geometry and is equipped with a Huber 512 Eulerian cradle and a solid state Ge detector. The insertion device is a high field wiggler with a critical energy of 26.5 keV at the minimum gap of 20 mm. A 1.5 mm copper filter cuts the spectrum below 50 keV, thereby minimizing the heat load on the monochromator crystal. The incident radiation with an energy in the range of 100 keV has a penetration depth of ~ 1 mm in YBCO samples. For monochromator and analyzer crystals either (2 0 0) SrTiO₃ crystals or (1 1 1) Si/TaSi₂ crystals³⁹ were used. Both types of crystals had a mosaic spread of $\sim 50''$ (arc seconds), resulting in a longitudinal resolution of 0.0075 \AA^{-1} at the (2 0 0) reflection of YBa₂Cu₃O_{6+x}. The transverse resolution is limited by the sample mosaicity, which was in the range of 0.05° - 0.1° for our samples, corresponding to $\sim 0.0015 \text{ \AA}^{-1}$ at the (2 0 0) reflection. The vertical resolution depends on the setting of the slits before and behind the sample. They were usually set to integrate the scattering over a quarter of a reciprocal lattice unit, that is 0.40 \AA^{-1} along the a and b axes and 0.13 \AA^{-1} along the c

axis. The sample was wrapped in Al-foil and mounted in a small furnace, designed for use in an Eulerian cradle. The furnace temperature was stable within 1°C. An inert atmosphere of 0.3 bar Ar was introduced into the furnace to prevent oxidation of the crystals. From the gas-volumetric preparations it is established that the reduction is negligible for temperatures below 300 °C, and we observed no changes in the structural properties that could be related to a change of oxygen composition during temperature cycling at temperatures below 250°C.

C. Analysis of superstructure data

The ortho-II superstructure reflections are well described by the scattering function

$$S(\mathbf{q}) = A/(1 + (q_h/\Gamma_h)^2 + (q_k/\Gamma_k)^2 + (q_l/\Gamma_l)^2)^y \quad (1)$$

where q_i , $i = h, k, l$ is the reduced momentum transfer and Γ_i the reduced inverse correlation length, related to the correlation length ξ_i by $\xi_h = a/(2\pi\Gamma_h)$ for the a direction and analogous along b and c . Equation 1 is a 3D anisotropic Lorentzian raised to the power y . The scattering function $S(\mathbf{q})$ has been convoluted with the resolution function, which is treated as a δ -function in the scattering plane and an integrating function in the perpendicular direction. The exponent y indicates the distribution of domain size, *i.e.* $y = 1$ points to an exponential decrease of the pair correlations as for example in the ramified clusters typically for critical fluctuations above the transition temperature. The exponent $y = 2$ may result from a domain size distribution around an average value Γ_i ⁴⁰ and, as mentioned in the Introduction, the asymptotic behaviour for large q is in agreement with Porod's law for scattering from 3D finite size domains with sharp boundaries. Furthermore Bray has shown that the tail of the scattering function from a topological defect of dimension m , in a system of dimension d is given by $S(q) \propto \frac{1}{q^{2d-m}}$ ⁴¹. The relation between Γ and the peak width (HWHM= Δ) is $\Delta/\sqrt{2^{1/y}-1}$. When full integration of the superstructure peak is performed perpendicular to the scattering plane by relaxing the vertical aperture the in-plane scattering function derived from Eq. 1 is described by a Lorentzian to the power $y' = y - \frac{1}{2}$.

The ortho-III, ortho-V and ortho-VIII superstructures are essentially 2D ordered giving rise to significant overlap of the peaks along l ^{23,25,26}. In this case full integration in the vertical direction cannot be obtained when the c axis is perpendicular to the scattering plane. For the 2D ordered superstructures with finite domain size and sharp boundaries it is expected that the scattering function in the ab plane should be a Lorentzian to the power $y' = y = 3/2$ because the integration along c is rather incomplete, whereas it should be a simple Lorentzian ($y' = y - 1/2 = 1$) when the c direction is in the scattering plane and full integration along the a or b direction is performed.

III. RESULTS

A. The ortho-II superstructure

The ortho-II phase is observed as a 3D ordered structure with anisotropic correlation length at compositions $0.35 \leq x < 0.62$ and no other superstructure was found in this range of oxygen content. Especially at $x = 0.35$ the q -space was surveyed unsuccessfully for correlations of the herringbone, $\sqrt{2}a \times 2\sqrt{2}a \times c$, or $2\sqrt{2}a \times 2\sqrt{2}a \times c$ type structures which were observed in other studies by electron^{10,13,42}, x-ray⁴³ and neutron diffraction¹⁴.

The largest correlation lengths are obtained for the ortho-II phase at $x = 0.50$. An example of the (2.5 0 0) superstructure reflection measured in crystal #1 is shown in Fig. 1. The crystal has been annealed by the thermal procedure marked 2 below. The room temperature properties of the oxygen superstructures are strongly dependent on the crystal quality and the thermal treatment. The four crystals labeled #1 - #4 in section II A have been prepared with $x = 0.50$, annealed at 500 °C for 6 days, cooled by 10 °C/hour to 100 °C where they were annealed for 36 hours and then quenched to room temperature. The diffraction studies were performed 5-10 days later. With this thermal treatment we assume, on the basis of the results presented below and in Ref. 44, that all the crystals have reached the late state of ortho-II domain growth, and the influence of the different room temperature annealing times is considered to be small compared to the differences due to impurities and defects.

Although it is possible to determine the impurity level in the crystal, it is often not known on which lattice sites the various impurities are located and what influence they have on the oxygen ordering. However, a crystal prepared as described in Ref. 36 using Al₂O₃ as crucible material resulted in a crystal with 6 mole % Al, which by neutron diffraction studies was found to be located on the Cu(1) site in the basal plane⁴⁵. This crystal did not show ortho-II superstructure ordering when it was prepared with $x = 0.50$. The nature and influence of lattice defects are equally difficult to quantify. One way to measure the overall quality of the crystal lattice is the mosaicity, *i.e.* the width of the rocking scan of the sample. Fig. 2 shows the HWHM of h, k and l scans obtained at room temperature of the ortho-II superstructure reflection versus the mosaicity for the four crystals #1 - #4. The h and l scans are measured in the ac scattering plane, and the scan along k in the ab plane. In both cases a full integration of the respective vertical widths, Δk and Δl is performed. It is immediately obvious that crystal #3 prepared with low purity chemicals have the largest mosaicity and the broadest ortho-II peaks. Thus, the purity of the chemicals is crucial for the development of large ortho-II domains. For crystals #1, #2 and #4 a linear relation between mosaicity and the HWHM of the ortho-II superlattice peak is found, with small deviations

of the width along h . With the mosaicity as a criteria of crystal quality crystal #1 is the most perfect one. This is corroborated by magneto-optic studies of the magnetic flux flow in the crystals. Crystal #1 is the only one that shows flux flow instability, which is considered to be a signature of very high crystal quality⁴⁶.

The influence of the thermal treatment has been studied in crystal #1. After the preparation for $x = 0.50$ mentioned above the crystal has been annealed the following six ways:

1. 70 days annealing at 80°C, cooling to room temperature in steps of 1°C/hour
2. 5 hours annealing at 100°C, quenched to room temperature and stored for 10 days
3. quenched from 170°C to room temperature and stored at room temperature for 97 days
4. cooled down from 170°C to room temperature in steps of 10°C every 10 minutes
5. cooled down from 170°C to room temperature with 4°C/minutes
6. quenched from 170°C to room temperature within 3 minutes

In Fig. 3 the normalized peak intensity is plotted versus the inverse correlation lengths measured at room temperature at the (2.5 0 5) superstructure reflection for the differently treated samples. The normalization of the peak intensity is made relative to the background. As mentioned above, the h and l scans are measured in the ac plane, the scans along k in the ab plane, and a full integration along the vertical widths is performed. The relation between the measured peak intensity and the peak widths in all three directions follows a quadratic dependence as indicated by the lines. This shows that the ratios between the line-widths Γ_h/Γ_k and Γ_l/Γ_k are independent of the thermal treatment. Further, since the measured peak intensity, I_{peak}^{obs} , includes an integral over the direction perpendicular to the scattering plane we establish that also the total integrated intensity, I_{int} , is independent of thermal treatment. This is easily seen from Fig. 3 and the following relations, where the integration is assumed to be along k :

$$I_{int} \propto I_{peak} \Gamma_h \Gamma_k \Gamma_l$$

$$I_{peak}^{obs} \propto I_{peak} \Gamma_k \propto I_{int} / (\Gamma_h \Gamma_l) \propto I_{int} / \Gamma_h^2$$

Accordingly, only the correlation length of the superstructure and thereby the characteristic domain size depend on the sample treatment. This indicates that the finite size domains have internal thermodynamic order and fill the crystal. Studies of the time dependent oxygen ordering following a temperature quench from the ortho-I into the ortho-II phase at this composition confirm that

the integrated intensity depends only on the temperature. These results will be published elsewhere⁴⁴.

It is instructive to consider the temperature variation of the ortho-II structure for crystal #1 prepared by thermal treatment 1. The phase transition from the ortho-II phase into the ortho-I phase was studied by means of ω -scans at the (2.5 0 5) reflection during initial heating and at subsequent cooling within one hour. The result is shown in Fig. 4. Clearly, the peak intensity is lower and the ω width is larger on cooling than on heating. However, the integrated intensity calculated as $I_{peak}^{obs} \times \omega^2$ is found to be the same during heating and cooling. Since the results of the ortho-II superstructure ordering indicate that internal superstructure order is established inside the finite size domains it is appropriate to define a transition temperature, T_{OII} . Several criteria may be used. Firstly the variation of the peak intensity of the superstructure reflection plotted in the top part of Fig. 4 shows an inflection point at 95°C, as determined by the minimum of the normalized slope (N.S.) of the peak intensity, plotted in the inset. The inflection point of the peak intensity indicates the cross-over from static order to critical fluctuations, *i.e.* the transition temperature T_{OII} . Secondly the onset of the line broadening of the superstructure reflection also marks the transition temperature. The temperature dependence of the line width above the transition can be well described by the critical exponent $\nu = 0.63$ for the 3D Ising model:

$$\Delta(T) = \Delta_0^\pm |T - T_c|^\nu \quad , \quad (2)$$

where Δ_0^\pm are the slopes below and above the transition temperature. This behavior is shown in the middle part of Fig. 4. From the fit to the heating data in the critical region we find $T_{OII} = 95$ °C. Thirdly the line shape changes from approximately a Lorentzian squared, *i.e.* $y' = \frac{3}{2}$, at room temperature to a simple Lorentzian at the transition temperature: $T_{OII} = 95$ °C shown in the bottom part of Fig. 4. A line shape described by a simple Lorentzian is characteristic for critical fluctuations above the transition temperature. During cooling a drastic slowing down of the ordering process is observed at temperatures close to the transition temperature as seen in the variation of the peak intensity, which starts to deviate from the heating data at ~ 105 °C.

The variation of the peak intensity and the peak width with temperature leads to the distinction of three areas during the heating cycle. Between room temperature and 50°C both the peak intensity and the width of the superstructure reflections are constant, *i.e.* both the domain size and the integrated intensity, which is a measure of the order parameter of the ortho-II phase, are constant within the time period studied. Between 50°C and 95°C the width of the superstructure reflections is still constant, but the peak intensity decreases with increasing temperature, indicating that the ortho-II order inside the domains and thereby the number of oxygen atoms ordered in alternating full and empty chains start to decrease. Finally, the increasing width and the decreasing

intensity in the temperature range above 95°C indicate the area of critical fluctuations above the transition temperature. This range is well described by the critical exponents. In contrast, the behavior below the transition temperature shows substantial deviations from what is expected from a regular second order phase transition, where a long range ordered phase should be formed.

The investigation of the temperature dependence of the ortho-II phase at $x = 0.42$ exhibits exactly the same behavior as found at $x = 0.50$ with a small shift in the transition temperature. Thus a stoichiometric oxygen content is only of minor importance for the behavior at the ortho-I/ortho-II phase transition. However, the peak widths, $\Delta h = 0.031(1)$, $\Delta k = 0.010(1)$, $\Delta l = 0.14(1)$, are significantly larger than found for the high purity crystal #1 with $x = 0.50$, *cf.* Figs. 2 and 3.

B. The ortho-III structure

The ortho-III phase is found at the oxygen compositions of $x = 0.72, 0.77$ and 0.82 . A crystal prepared with $x = 0.87$ showed no sign of any oxygen ordering. At these oxygen compositions the ortho-III phase is formed by the sequence (110) of two full chains and one empty chain. Accordingly, the size of the unit cell is tripled along a and the diffraction pattern shows two superstructure reflections along h between the fundamental Bragg peaks. As shown in Fig. 5 the ortho-III super lattice peaks are well defined in the ab plane, but like all superstructures due to oxygen ordering in YBCO, broadened due to finite domain sizes. In contrast to the ordering in the ab plane, the l -dependence of the diffracted intensity shows only a broad modulation, with a peak width corresponding to more than one reciprocal lattice unit. This l -modulation is characteristic of the ortho-III structure and has been found in all samples exhibiting the ortho-III phase^{23,25,26}, which indicates that the ordering of oxygen atoms takes place in the ab -plane, whereas different planes are only weakly correlated. Thus, in contrast to the ortho-II structure, which is 3D ordered, the ortho-III phase is essentially a 2D ordered superstructure. As mentioned in Section II C a simple Lorentzian is expected for scattering from finite size domains in a 2D system when the integration of the peaks is performed either along the a or the b direction ($y' = y - 1/2 = 1$), whereas a Lorentzian to the power $y' = y = 3/2$ is expected for integration along l . However, the peak shapes along h and k are well described by Lorentzians, independent of which component is integrated in the vertical direction. Attempts to include a variable power y did not improve the fits when the l direction was vertical. The smallest widths, which have been reported previously by Schleger *et al.*²⁶ are found in the $x = 0.77$ crystal with $\Delta h = 0.031(1)$ and $\Delta k = 0.0090(2)$.

One example of the temperature dependence of the ortho-III phase is shown in Fig. 6 for the crystal with

composition $x = 0.72$. Here the (8/3 0 5) reflection was scanned along h at various temperatures. Similar to the transition of the ortho-II phase the peak intensity and peak width are frozen at temperatures smaller than 35°C. Above this temperature critical fluctuations are observed. Fitting the temperature dependence of the peak width a critical exponent of $\nu = 0.92(8)$ is obtained, with a transition temperature of $T_{OIII} = 48(5)^\circ\text{C}$. This value for the critical exponent is in good agreement with the theoretical value of $\nu = 1$ for the 2D Ising model and confirms the 2D character of the ordering.

C. Ortho-V

The investigation of a crystal prepared with the oxygen composition of $x = 0.62$ shows a mixture of ortho-II and ortho-V phase at room temperature. This is revealed by the observation of diffuse peaks at positions of $h = 2.4, 2.5$ and 2.6 as shown in Fig. 7. The peak at $h = 2.5$ results from the ortho-II structure, and the peaks at $h = 2.4$ and $h = 2.6$ are consistent with a unit cell which is enlarged five times in the a direction, *i.e.* the ortho-V structure. The two small peaks seen in the h -scan in Fig. 7 at $h=2.23$ and $h=2.83$ are an Al-powder line and possibly a grain of an unknown phase oriented with the lattice, respectively. The hump at $h=2.83$ has also been observed when the same crystal was prepared with other oxygen stoichiometries (compare with Fig. 9 and Ref. 26). A similar diffraction pattern, consistent with a mixture of ortho-II and ortho-V has been observed in all ($h 0 l$) scans performed with $1 \leq h \leq 4$ and $l=0,3,5,6,7$ (8 scans in total). However, none of these scans showed a peak at position $\vec{Q} = (\frac{1}{5} 0 l)$. This is explained by the structure factor calculations of the superlattice peaks from the ideal ortho-V ordering sequence (10110) shown in Ref. 47. The intensities of the peaks at $(1/5 0 0)$ are indeed much smaller than the ones at $(2/5 0 0)$ and $(3/5 0 0)$. However, this model takes into account only the oxygen order, and, as discussed in Section I, the superlattice peaks are caused by both the oxygen order and the cation displacements. These displacements and the pronounced disorder may change the intensities and reduce them further.

Due to the heavy overlap of the peaks from the two phases it is difficult to determine the peak shape and width. However, analysis of the ortho-II and ortho-V peaks using Lorentzian profiles gave the following HWHM in reciprocal lattice units at room temperature: $\Delta h = 0.040(28)$, $\Delta k = 0.0078(16)$, $\Delta l = 0.12(3)$ for ortho-II, and $\Delta h = 0.058(10)$, $\Delta k = 0.0096(19)$ for ortho-V. The scan along l at $(2.5 0 l)$, shown in Fig. 7, exhibits the intensity modulation well known for 3D ordering in the pure ortho-II phase, but the heavy overlap of the peaks prevents that the 2D short range type of modulation expected for the ortho-V peaks along l can be determined independently.

The temperature dependence of this mixed phase was measured by h -scans between the (2 0 0) and the (3 0 0) Bragg reflections and the diffraction pattern was fitted to three Lorentzians with fixed positions at 2.4, 2.5 and 2.6. Looking at the measurement of the phase transition of this mixed phase, shown in Fig. 8, one observes that the ortho-V correlations disappear between 50°C and 70°C and at the same time the ortho-II gains intensity. Also during the cooling cycle the ortho-II correlations dominate the diffraction pattern. The ortho-II correlations disappear at approximately 110 °C. Both facts together with our knowledge about the ordering kinetics^{8,44} indicate that during the cooling process the ortho-II phase is stabilized at higher temperature than ortho-V and with rather fast ordering kinetics. Then at lower temperature the ortho-V phase becomes stable, but due to the slow ordering kinetics at this lower temperature the ortho-V domains do not form within the one hour time period of the experiment.

D. Ortho-VIII

Figure 9 shows h , k and l scans for the oxygen composition $x = 0.67$. The left part with h scans along (h 0 0) with $2 < h < 3$ reveals diffuse superlattice peaks at $h = 2.382(4)$ and $h = 2.627(3)$. The peak positions and profiles have been fitted to two Lorentzians giving a HWHM of $\Delta h = 0.053$. The middle part shows that the peaks are also localized in the transverse direction with a width of $\Delta k = 0.013(2)$. The modulation of the intensity for a scan along l (right part of the figure) has a similar q dependence as the corresponding scan for the ortho-III phase, shown in Fig. 5. Thus, there are no well-defined peaks along l , indicating essentially 2D ordering with substantial disorder in the stacking of full and empty chains along the c direction. Similar superlattice peaks have been observed at positions in reciprocal space of (h 0 3) and (h 0 5) with $2 \leq h \leq 3$. The superstructure peak positions at modulation vectors with $nh_m = 0.382$ and 0.627 are close to the expected values $nh_m = 3/8$ and $5/8$ for a superlattice with a unit cell of $8a \times b \times c$, *i.e.* the ortho-VIII phase. The expected sequence of full and empty chains of the ideal ortho-VIII structure is (11010110). Calculating the intensities of the superlattice peaks for this ideal case one finds that the observed peaks at $nh_m = 3/8$ and $5/8$ are the strongest, the peaks at $nh_m = 2/8, 4/8$ and $6/8$ are about one order of magnitude smaller, and the ones at $nh_m = 1/8$ and $7/8$ are about two orders of magnitude smaller (compare with the presentation in Ref. 47). Due to the weak ordering it is unlikely that the smaller superlattice reflections can be observed.

The temperature dependence was observed from h -scans at the ($2\frac{3}{8}$ 0 3) peak position and the results are shown in Fig. 10. The onset of broadening of the superstructure peaks takes place at $T_{OVIII} = 42(5)$ °C. The

temperature dependence of the peak width above the transition temperature is described by the critical exponent of $\nu = 0.79(3)$ as shown in the middle part of Fig. 10. This value is between the exponent of 0.63 for the 2D and 1 for the 3D Ising model. Another interesting feature of this phase transition is revealed by the inspection of the peak position. When the temperature exceeds 50 °C the peak position changes continuously from $h = 2.372$ to $h = 2.4$ which corresponds to the position of the ortho-V phase. Above 90°C the peak shifts gradually to $h = 2.33$ at 150°C, the location of the peaks of the ortho-III structure. Upon cooling the data are reproduced down to 75°C, at lower temperatures the intensity is significantly reduced and the structure freezes into the ortho-V phase.

E. The oxygen ordering phase diagram

From the transition temperatures obtained in the present and previous studies^{8,19,26} using hard x-ray diffraction and the same type of crystals we may establish phase lines for the oxygen superstructure ordering. Combining these data with the transitions temperatures, T_{OI} , of the phase transition from the tetragonal to the orthorhombic ortho-I phase, obtained by neutron powder diffraction¹, we may construct the structural phase diagram of oxygen ordering in YBCO, shown in Fig. 11. In the figure is also included the phase transition temperatures, T_{OI} and T_{OII} predicted by Monte Carlo simulations⁴⁸ based on the ASYNNNI model⁴⁹ with *ab initio* interaction parameters⁵⁰.

The only true equilibrium structures are the ortho-I phase and the tetragonal phase, all superstructures formed by oxygen ordering do not show long range ordering. Within the temperature range studied the tetragonal phase is the only one observed for $x < 0.35$. Below the tetragonal to orthorhombic phase transition temperature the 3D ordered ortho-I phase always develops, and it is the only structure observed for $x > 0.82$. For $0.35 \leq x < 0.62$ the 3D short range ordered ortho-II phase is the only stable superstructure. Similarly, a single phase ortho-III structure with 2D finite size ordering is observed for $0.72 \leq x \leq 0.82$. At intermediate compositions a mixed phase of ortho-II and ortho-V is found at $x = 0.62$, and ortho-VIII is found at $x = 0.67$ in crystals that have been slowly cooled to room temperature as described in Sec. II A. Both the ortho-V and the ortho-VIII structures are essentially 2D ordered and have finite size ordering. During heating the ortho-V structure transforms into ortho-II and it does not recover on cooling within one hour. Above room temperature the ortho-VIII structure transforms gradually first into ortho-V and then into ortho-III. On subsequent cooling the ortho-V superstructure is recovered and remains stable within the one hour time period of the measurements.

The line shape of the superstructure reflections is in

most cases well described by a simple Lorentzian ($y = 1$). Only for the ortho-II phase between $0.42 \leq x < 0.62$ a Lorentzian squared shape ($y = 2$) is found. At the low oxygen side of the ortho-II phase $x \leq 0.36$ the small peak to background ratio (see bottom part of Fig. 12) does not permit the determination of the exponent of the Lorentzian. The domain size of the superstructures depends strongly on the crystal quality and the annealing times. However, for high quality crystals that have been annealed by the standard procedure for studies of the phase diagram (described in Sec. II A) we expect that the domains are at the late state of growth and therefore only weakly time dependent (*cf.* Fig. 3, thermal preparations 1 and 2, and Refs. 8 and 44). On this basis we consider the results presented in Sec. III of the peak widths measured at room temperature after the initial thermal preparation as saturation values. The HWHM of the superlattice peaks measured along the three axis of reciprocal space as function of oxygen composition is depicted in Fig. 12 (top). The parallel lines (guides to the eye) in the logarithmic plot observed in the ortho-II phase as well as in the ortho-III phase show that the ratio of the anisotropy is constant within a given structural phase. For the ortho-II phase we find the following ratios of the inverse correlation lengths at room temperature: $\Gamma_h/\Gamma_k = 2.7(6)$ and $\Gamma_l/\Gamma_k = 15(2)$. The ab plane ratio seems to be independent also of the type of structure, since the ratio for the ortho-III phase: $\Gamma_h/\Gamma_k = 2.9(4)$ is in good agreement with the value of the ortho-II phase. This implies that the domain pattern in the ab plane scales in both the ortho-II and the ortho-III phases, and in ortho-II the scaling is extended to 3D. The peak intensities cannot be compared directly because different crystals and instrumental settings have been used. However, the peak intensity normalized to the background, shown in the bottom part of Fig. 12, is essentially an independent parameter of the ordering properties. From this normalized peak intensity and the HWHM data it is clear that the optimal superstructure order parameter is found close to $x = 0.55$.

The oxygen composition x of all the ordered phases deviates systematically from the ideal composition of these phases. For example the longest correlation lengths for the ortho-II phase are likely to be at $x \simeq 0.55$. Unfortunately no data points are available at this composition. Theoretically one would expect the best ortho-II order for $x = 0.50$. This deviation is even more significant for the ortho-III phase, which is expected at $x = 0.67$, but observed around $x \simeq 0.77$. Thus, the deviation from the ideal composition increases with increasing chain density and the amount of oxygen atoms occupying sites on the empty chains at room temperature can be estimated to be about 10 % for ortho-II and 30 % for ortho-III.

IV. DISCUSSION

A. Experimental results

It has been known for several years that the ortho-II and ortho-III superstructures are bulk structural phases of finite size domains. Several other superstructures have been suggested, mainly from electron microscopy. In the present paper we have shown that also the ortho-V and ortho-VIII correlations observed by electron microscopy result from bulk structural ordering, but we found no evidence for the ortho-IV phase. However, we recognize in particular the early electron microscopy results obtained by Beyers *et al.*¹² which are in close agreement with our room temperature data. Beyers *et al.* observe the ortho-II and ortho-III superstructures in the same composition range as in our studies. Furthermore, they found co-existence of ortho-II and ortho-V at $x = 0.65$, and a structure similar to the ortho-VIII phase, which they call a '(0.37 0 0)' structure, at $x = 0.71$.

Beyers *et al.* attributed the clear disagreement between the observed oxygen compositions and the stoichiometries of the ideal superstructure phases to gradients in the oxygen content of the sample, which might be different on the surface and in the bulk material. In our experiment such differences can be ruled out. We conclude that this deviation is an intrinsic property of the oxygen ordering mechanism. It is possible that the phase lines between the superstructure phases are in fact tilted, and only at zero temperature the ideal oxygen stoichiometry of the superstructure phases is found. However, this will never happen because the oxygen ordering kinetics is very slow at the temperatures where the superstructures become stable, and the movement of Cu-O chains freeze effectively below approximately 40 °C.

Beyers *et al.* interpret the mixing of ortho-II and ortho-V phases at $x = 0.65$ as a phase separation, which leads to the 60 K plateau¹². Our investigation of the temperature dependence together with the studies of the ordering kinetics^{8,44} may lead to a different conclusion. During the cooling of a sample with an oxygen content of $x = 0.62$ (in the case of Beyers *et al.* $x = 0.65$) oxygen starts to order in the ortho-II phase. The relatively high temperature enables a fast growth of ortho-II domains. At lower temperature the ortho-V phase becomes stable, but now at temperatures just above room temperature where the growth of ortho-V domains is slow. A full transformation into the ortho-V phase cannot be precluded but it is very time consuming. Therefore, we suggest that domains of the complex ortho-V superstructure start to grow inside the ortho-II structure and a mixed phase, rather than phase separation, results.

From studies of the oxygen ordering properties it has become clear that the finite size of the ortho-II superstructure results from formation of anti-phase boundaries that limit the domain growth due to slow kinetics of moving long Cu-O chains. The reason for this has been discussed by Schleger *et al.*⁸, and it was speculated that random fields introduced by impurity defects in the

crystal stabilize the anti-phase domain walls and prevent formation of long range order. This is corroborated by the present studies and additional studies of the ordering kinetics⁴⁴. However, the observation of superstructures extending over eight unit cells shows the importance of long range interactions for the ordering mechanism. That these long range interactions play a significant role for the finite size ordering has recently been established by model simulations³³, and will be discussed further below. For the ortho-III, ortho-V and ortho-VIII superstructures the small 2D domains indicate that the ordering resembles a random faulting sequence of ortho-II and ortho-III. Khachatryan and Morris⁵¹ have suggested that this is a likely ordering scheme, and they have calculated structure factors which are qualitatively similar to those observed at room temperature in our experiments. However, the fact that the ortho-V and ortho-VIII superstructures only appear when they are slowly cooled indicates that the long range interactions tending to form these superstructures become effective at low temperatures, but the slow oxygen ordering kinetics for movement of long Cu-O chains prevent that well-defined domains are formed. As mentioned in Sec. II C we would expect a diffraction profile of a Lorentzian to the power $y' = y = 3/2$ from 2D domains with sharp boundaries when the integration along the c axis is incomplete. The observation that all the superstructure peaks of the ortho-V, ortho-VIII and ortho-III peaks are described by Lorentzian profiles suggests that these superstructures have a more fuzzy type of boundaries than the ortho-II domains.

Generally, there is significant hysteresis in the superstructure ordering when the temperature is cycled through the phase transitions. The ortho-II and ortho-III superstructures are re-established during cooling from the ortho-I phase within one hour. However, the ortho-V phase (mixed with ortho-II) and the ortho-VIII do not recover during cooling within this short time period. Instead, the less complex superstructures, ortho-II and ortho-V develop, respectively. It is obvious that the superstructure ordering does not represent equilibrium phases, and it cannot be precluded that more complex superstructures may be formed by very long time annealing at an appropriate temperature or in crystals that are even more perfect than the present ones. According to Ostwald's step rule for phase transformations, metastable phases may be formed, before the system finally transforms into the stable phase, as long as nucleation centers with a similar structure like the metastable phases are present. In our case the ortho-II and ortho-III phase might be nucleation centers for the ortho-V phase, which in turn, at $x = 0.67$, is metastable and serves as a nucleation center for the ortho-VIII phase (see figure 10). Thus, although we have been able to define unique transition temperatures, at least for the ortho-II superstructure phase, it is questionable whether we have established a phase diagram in the usual sense. This may explain why the phase diagram does not comply with Gibb's phase

rule.

The 3D ordered superstructures with unit cells $2\sqrt{2}a \times 2\sqrt{2}a \times c$ and $\sqrt{2}a \times 2\sqrt{2}a \times c$, the so called herringbone structure, have been observed by electron microscopy, and one group has reported on these structures by neutron¹⁴ and x-ray⁴³ diffraction techniques on single crystals with composition $x = 0.35$. However, no other experiments with bulk structural techniques, could confirm these results. Bertinotti *et al.*⁵² and Yakhou *et al.*⁵³ have shown that the reflections of the herringbone type can be assigned to BaCu_3O_4 grains in the crystals. Krekels *et al.*^{54,55} attribute the $2\sqrt{2}a \times 2\sqrt{2}a \times c$ structure to distortions of the CuO_5 pyramids in the CuO_2 planes, and Werder *et al.*⁵⁶ suggest that they could result from ordering of copper and barium vacancies in the lattice. The consensus from these and several other studies is therefore that the $2\sqrt{2}a \times 2\sqrt{2}a \times c$ and the herringbone type structures are not oxygen ordering superstructures in YBCO. If they were, it is peculiar that they have 3D long range order while the Cu-O chain ordering develops only finite size domains. Also, we have found no evidence of them at any composition x in the present hard x-ray diffraction studies on carefully prepared high quality single crystals.

B. Significance for superconductivity

The significance of the oxygen ordering for charge transfer and superconductivity is obvious from many studies. Chemical bond considerations combined with structural⁵⁷ and spectroscopic studies^{58,59} have shown that the basal plane copper in undoped $\text{YBa}_2\text{Cu}_3\text{O}_{6+x}$, ($x = 0$), is monovalent and that simple oxygen monomers, *i.e.* Cu-O-Cu, will not give rise to charge transfer. However, charge transfer is observed for larger x where Cu-O chains are formed. Cava *et al.*⁵⁷ and Tolentino *et al.*⁵⁸ have established that an increasing amount of oxygen give rise to a charge transfer to the CuO_2 planes that is in good agreement with the well-known plateau variation of T_c with $T_c = 58$ K around $x = 0.5$ and $T_c = 93$ K close to $x = 1$. Relating the oxygen ordering to the variation of T_c observed *e.g.* by Cava *et al.*⁵⁷ we find that the 58 K plateau is identical to the stability range of the ortho-II superstructure, the rise in T_c from the 58 K to the 93 K plateau takes place at values of x where the ortho-V/II, ortho-VIII and ortho-III structures are found, and the 93 K plateau coincide with the oxygen compositions of the ortho-I phase.

The significance of the ortho-II ordering for superconductivity has been shown directly by Veal *et al.*⁵ and Madsen *et al.*⁷. Both groups have shown that T_c is significantly reduced just after a quench and increases with time towards the equilibrium values with a thermal activated time constant. The conclusion, that may be drawn from these experiments and the present structural data, is that the formation of ortho-II superstructure is deci-

sive for the charge transfer and T_c . When the sample is quenched from temperatures above T_{OII} , and even from the tetragonal phase, it is only the time used to quench it into the ortho-II phase that matters. A time dependent increase of T_c is observed at annealing temperatures down to 250 K. Most likely this temperature is the lower limit for local oxygen jumps which dominates the oxygen ordering at the very early time. It is unlikely that the domain wall separating anti-phase domains are mobile at 250 K.

C. Relation to model calculations

There has been many theoretical studies of the oxygen ordering in YBCO and attempts to correlate the structural ordering with the electronic properties and superconductivity. These include phenomenological relations between ordered oxygen domains and T_c ^{60,61}, and electron band structures calculated from oxygen chain configurations estimated *ad hoc*⁶² or derived from model studies⁶³. More realistic and elaborate models, where the electronic degrees of freedom from the strongly correlated electron system has been included in combination with the oxygen ordering properties, have also been considered^{64–66}. The aim is clearly to understand details of the local oxygen ordering properties which are important for the electronic structure and the charge transfer, but difficult to obtain directly from experiments. The predictive power of these model studies for the structural and electronic properties is strongly related to their ability to reproduce the experimental findings, as presented in the present structural studies.

Most of the structural models are based on local effective oxygen-oxygen interactions in a 2D lattice gas formulation^{49,67}. These models do not take into account long range interactions like strain effects and will therefore not reproduce the twin domain formation observed experimentally at the onset of the ortho-I ordering. Models including such long range interactions have been considered⁶⁸. It has also been suggested that the diffuse scattering results from generation of (1 0 0) interstitial plane defects that order by forming a Magneli type homologous series⁶⁹. However, the oxygen ordering observed experimentally has a predominant 2D character related to the CuO_x basal plane, that is (0 0 1) planes. It takes place inside the ortho-I twin domains and has domain sizes that are usually much smaller than the twin domains. Strain effects and long range Coulomb type interactions are therefore of little significance for the oxygen superstructure formation but they do play a role for the mesoscopic ordering properties.

The simplest model, that accounts for many elements of the oxygen ordering properties, like the formation of Cu-O chains and the presence of the tetragonal, ortho-I and ortho-II phases, is the so-called ASYNNNI (Asymmetric Next Nearest Neighbor Ising) model⁴⁹. The

ASYNNNI model is a 2D lattice gas (or Ising) model with effective oxygen-oxygen pair interactions, that are assumed to be independent of temperature and composition x . The interactions parameters include a strong Coulomb repulsion V_1 between the oxygen atoms on nearest neighbor sites and an attractive covalent interaction V_2 between oxygen atoms that are bridged by a Cu atom. These two interactions locate the oxygen on the b axis (the O(1) site) and prevent significant oxygen occupation on the a axis (the O(5) site) in the orthorhombic phases at moderate temperatures and compositions $x > 0.35$. A weaker effective repulsive Coulomb type interaction V_3 between oxygen atoms that are next nearest neighbors and not bridged by a Cu atom stabilizes the ortho-II superstructure. The ASYNNNI model accounts quantitatively⁴⁸ for the temperature and composition dependence of the experimental structural phase transition between the tetragonal and the ortho-I phases¹ (see Fig. 11) by use of interaction parameters, which are consistent with values obtained by Sterne and Wille⁵⁰ from first principles total energy calculations: $V_1/k_B = 4278$ K, $V_2/k_B = 1488$ K and $V_3/k_B = 682$ K. It also predicts the existence of the ortho-II phase, but it cannot account for the additional superstructure phases, ortho-III, ortho-V and ortho-VIII. Moreover, it predicts long range order of the superstructure phases, which has never been obtained experimentally, and it cannot account quantitatively for the ortho-I to ortho-II phase transition temperature.

Extensions of the ASYNNNI model have been suggested to account for the shortcomings. These include an effective 3D interaction with a nearest neighbor attractive interaction along c that is $V_4 \approx -0.02V_1$ ⁴⁸, effects of electronic degrees of freedom in the Cu-O chain structure, as mentioned above^{64–66}, and 2D Coulomb type interactions of longer range than V_2 and V_3 ^{47,71}. For the 2D ordering it has been argued that a single additional interaction parameter for oxygen atoms that are $2a$ apart and not bridged by copper should be sufficient³³. This is corroborated by an estimate of screened Coulomb potentials which shows that the interaction between oxygen atoms separated by $2a$ is of the order of $V_5 = 0.02V_1$, and it decays rapidly for larger distances. At the temperature where V_5 becomes effective Cu-O chains have already been formed³³ and it will act as an effective interaction between chains rather than between oxygen pairs. The V_5 interaction stabilizes the ortho-III phase by construction but it is not expected to account for the ortho-V and ortho-VIII phases. The influence of including effective Coulomb type Cu-O chain interactions extending beyond a and $2a$ has been studied analytically in the framework of a 1D Ising model⁴⁷. Here a sequence of branching phases develops for $T \rightarrow 0$ in order to comply with the Nernst principle and stoichiometric phases at different compositions x . However, for the YBCO system it is expected that the interactions of range beyond $2a$ play a role only at low temperatures where effectively the structural ordering is frozen. Also, the projection to a 1D system requires that rather long Cu-O chains are formed,

and recent Monte Carlo simulations have shown that finite chain lengths may result when the ASYNNNI model is extended by the V_5 interaction, even for $T \rightarrow 0$ ³³. On the other hand, the ASYNNNI model extended this way predicts that the V_5 parameter is sufficient to establish not only short range correlations of ortho-V and ortho-VIII but also the ortho-II and ortho-III superstructures do not develop long range order, as observed experimentally. The finite size ordering of the superstructures is therefore not necessarily a consequence of impurities or defects that pin the domain walls, but may be an intrinsic disordering property. Experiments on even more perfect crystals than used in the present study could supply additional information about the influence of defects on the ordering properties. In further agreement with the experiments, the ASYNNNI model extended with the V_5 as well as the 3D V_4 parameters predicts a significant suppression of the T_{OII} ordering temperature relative to the T_{OI} temperature which the original version failed to do (see Fig. 11). It is therefore, a promising model for analysis of experimental results and credible predictions about the local oxygen ordering properties. So far the theoretical phase diagram including the V_4 and V_5 interactions has not been determined. The present experimental results can be used as a guide to further model studies. Here it is interesting to note that our data show that the ratios of the correlation lengths are essentially independent of the oxygen stoichiometry in the ortho-II and the ortho-III phases. A comparison between this result and mean field predictions of the peak widths⁴⁰ indicates that the ASYNNNI model interaction parameters are independent of x . This assumption has been a major objection against the validity of the ASYNNNI model.

V. CONCLUDING SUMMARY

High energy X-ray diffraction has proven to be a unique tool for studies of oxygen ordering properties in the orthorhombic phase of YBCO. Chain ordered superstructures of the ortho-II, ortho-III, ortho-V and ortho-VIII types have been observed in high quality single crystals with this bulk sensitive technique. None of the superstructures develops long range order. Only the ortho-II phase is a 3D ordered superstructure with anisotropic correlation lengths. The ortho-II correlation lengths observed at room temperature depend on the oxygen composition (optimal for $x = 0.55$), crystal perfection and thermal annealing. All other superstructures have 2D character with ordering only in the ab -plane. The ratio of the ab plane correlation lengths is essentially independent of the oxygen composition and whether the ordering is ortho-II or ortho-III. The transition temperatures of the superstructures are between room temperature and 125°C. The ordering properties resulting from thermal cycling through the T_{OII} and the T_{OIII} ordering temperatures show that finite size domains with inter-

nal thermodynamic equilibrium are formed. The domain size observed on cooling from the ortho-I phase within one hour is significantly reduced compared to the value obtained by long time annealing. The observation of ortho-V mixed with ortho-II, and ortho-VIII superstructures shows that these superstructures are bulk properties, and that Coulomb interactions beyond next-nearest-neighbors become effective close to room temperature. The ordering of the ortho-V and ortho-VIII superstructures does not reproduce when the sample is cooled from the ortho-I phase within one hour, and it can not be precluded that additional superstructure phases may be formed by careful annealing of high quality single crystals. Therefore, although an unambiguous criterion has been identified for the ordering temperatures of the finite size ortho-II and ortho-III superstructures, the resulting 'phase diagram' is not an equilibrium phase diagram in the usual sense.

ACKNOWLEDGMENTS

This work was supported by the EC TMR - Access to Large Scale Facilities Programme at HASYLAB, and the Danish Natural Science Research Council through Dan-Sync. The Danish Technical Science Research Council supports TF. Collaboration with H. Casalta, R. Hadfield and P. Schleger on initial studies preceding this work is gratefully acknowledged. Technical assistance from S. Nielsen, R. Novak, A. Swiderski and T. Kracht is much appreciated.

-
- * present address: Department of Physics, Brookhaven National Laboratory, Upton, New York 11973, USA
- ¹ N.H. Andersen, B. Lebech and H.F. Poulsen, *Physica C* **172**, 31 (1990).
 - ² P. Schleger, W. Hardy and B. Yang, *Physica C* **176**, 261 (1991).
 - ³ J.D. Jorgensen, M.A. Beno, D.G. Hinks, L. Soderholm, K.J. Volin, R.L. Ritterman, D.G. Grace, I.K. Schuller, C.U. Segre, K.Z. Zhang and M.S. Kleefisch, *Phys. Rev. B* **36**, 3608 (1987).
 - ⁴ H. Claus, S. Yang, A.P. Paulikas, J.W. Downey and B.W. Veal, *Physica C* **171**, 205 (1990).
 - ⁵ B.W. Veal, A.P. Paulikas, H. You, H. Shi, Y. Fang and J.W. Downey, *Phys. Rev. B* **42**, 6305 (1990).
 - ⁶ S. Libbrecht, E. Osquiguil, B. Wuyts, M. Maenhoudt, Z.X. Gao and Y. Bruynseraede, *Physica C* **206**, 51 (1993).
 - ⁷ J. Madsen, N.H. Andersen, M. v. Zimmermann and Th. Wolf, Annual progress report of the Department of Solid State Physics 1 January - 31 December 1996, page 47 (1997). Ris Report R-933 (EN).
 - ⁸ P. Schleger, R. Hadfield, H. Casalta, N.H. Andersen, H.F. Poulsen, M. von Zimmermann, J.R. Schneider, Ruixing

- Liang, P. Dosanjh and W.N. Hardy, Phys. Rev. Lett. **74**, 1446 (1995).
- ⁹ H.W. Zandbergen, G. van Tendeloo, T. Okabe and S. Amelinckx, Phys. Stat. Sol. **103**, 45 (1987).
- ¹⁰ J. Reyes-Gasga, T. Krekels, G. van Tendeloo, J. van Landuyt, S. Amelinckx, W.H.M. Bruggink and H. Verweij, Physica C **159**, 831 (1989).
- ¹¹ D.J. Werder, C.H. Chen, R.J. Cava and B. Batlogg, Phys. Rev. B **38**, 5130 (1988).
- ¹² R. Beyers, B.T. Ahn, G. Gorman, V.Y. Lee, S.S.P. Parkin, M.L. Ramirez, K.P. Roche, J.E. Vazquez, T.M. Gür and R.A. Huggins, Nature **340**, 619 (1989).
- ¹³ M.A. Alario-Franco, C. Chaillout, J.J. Capponi, J. Chenavas and M. Marezio, Physica C **156**, 455 (1988).
- ¹⁴ R. Sonntag, D. Hohlwein, T. Brückel and G. Collin, Phys. Rev. Lett. **66**, 1497 (1991).
- ¹⁵ Th. Zeiske, D. Hohlwein, R. Sonntag, F. Kubanek and Th. Wolf, Physica C **194**, 1 (1992).
- ¹⁶ R.M. Flemming, L.F. Schneemeyer, P.K. Gallagher, B. Batlogg, L.W. Rupp and J.V. Waszczak, Phys. Rev. B **37**, 7920 (1988).
- ¹⁷ V. Plakhty, B. Kviatkovsky, A. Stratilatov, Yu. Chernenkov, P. Burlet, J.Y. Henry, C. Marin, E. Ressouche, J. Schweizer, F. Yakou, E. Elkaim and J.P. Lauriat, Physica C **235-240**, 867 (1994).
- ¹⁸ E. Straube, D. Hohlwein and F. Kubanek, Physica C **295**, 1 (1998).
- ¹⁹ H.F. Poulsen, M. von Zimmermann, J.R. Schneider, N.H. Andersen, P. Schleger, J. Madsen, R. Hadfield, H. Casalta, Ruixing Liang, P. Dosanjh and W.N. Hardy, Phys. Rev. B **53**, 15335 (1996).
- ²⁰ J. Grybos, D. Hohlwein, Th. Zeiske, R. Sonntag, F. Kubanek, K. Eichhorn and Th. Wolf, Physica C **220**, 138 (1994).
- ²¹ P. Burlet, V.P. Plakhty, C. Marin and J.Y. Henry, Phys. Lett. A **167**, 401 (1992).
- ²² Th. Zeiske, R. Sonntag, D. Hohlwein, N.H. Andersen and Th. Wolf, Nature **353**, 542 (1991).
- ²³ V. Plakhty, P. Burlet and J.Y. Henry, Physics Lett. A **198**, 256 (1995).
- ²⁴ W. Schweiss, W. Reichardt, M. Braden, G. Collin, G. Heger, H. Claus and A. Erb, Phys. Rev. B **49**, 1387 (1994).
- ²⁵ V. Plakhty, A. Startilov, Yu. Chernenkov, V. Fedorov, S.K. Sinha, Chun L. Loong, G. Gaulin, M. Vlasov and S. Moshkin, Sol. State Comm. **84**, 639 (1992).
- ²⁶ P. Schleger, H. Casalta, R. Hadfield, H.F. Poulsen, M. von Zimmermann, N.H. Andersen, J.R. Schneider, R. Liang, P. Dosanjh and W.N. Hardy, Physica C **241**, 103 (1995).
- ²⁷ Th. Zeiske, D. Hohlwein, R. Sonntag, J. Grybos, K. Eichhorn and Th. Wolf, Physica C **207**, 333 (1993).
- ²⁸ D. Hohlwein in *Materials and Crystallographic Aspects of HTc-Superconductivity*, edited by E. Kaldis (Kluwer Academic Publishers, The Netherlands, 1994), p. 65.
- ²⁹ E. Straube, D. Hohlwein and F. Kubanek, Physica C **295**, 1 (1998).
- ³⁰ W. Scharz, O. Blaschko, G. Collin and F. Marucco, Phys. Rev. B **48**, 6513 (1993).
- ³¹ R.A. Hadfield, P. Schleger, H. Casalta, N.H. Andersen, H.F. Poulsen, M. von Zimmermann, J.R. Schneider, M.T. Hutchings, D.A. Keen, Ruixing Liang, P. Dosanjh and W.N. Hardy, Physica C **235-240**, 1267 (1994).
- ³² T. Frello, N.H. Andersen, J. Madsen, M. Käll, M. von Zimmermann, O. Schmidt, H.F. Poulsen, J.R. Schneider and Th. Wolf, Physica C **282-287**, 1089 (1997).
- ³³ D. Mønster, P.-A. Lindgård and N.H. Andersen, unpublished.
- ³⁴ E. Kaldis, J. Röhler, E. Liarokapis, N. Poulakis, K. Conder and P.W. Loeffen, Phys. Rev. Lett. **79**, 4894 (1997).
- ³⁵ R. Liang, P. Dosanjh, D.A. Bonn, D.J. Baar, J.F. Carolan and W.N. Hardy, Physica C **195**, 51 (1992).
- ³⁶ Th. Wolf, W. Goldacker, B. Obst, G. Roth and R. Flükiger, J. Crys. Growth **96**, 1010 (1989).
- ³⁷ H. Casalta, P. Schleger, P. Harris, B. Lebech, N.H. Andersen, R. Liang, P. Dosanjh and W.N. Hardy, Physica C **258**, 321 (1996).
- ³⁸ R. Bouchard, D. Hupfeld, T. Lippmann, J. Neufeind, H.-B. Neumann, H.F. Poulsen, U. Rütt, T. Schmidt, J.R. Schneider, J. Süßenbach and M. von Zimmermann, Synchrotron Radiation News **5**, 90 (1998).
- ³⁹ H.-B. Neumann, J.R. Schneider, J. Süßenbach, S.R. Stock and Z.U. Rek, Nuclear Instrum. Methods A **372**, 551 (1996).
- ⁴⁰ T. Fiig, N.H. Andersen, J. Berlin and P.A. Lindgård, Phys. Rev. B **51**, 1226 (1995).
- ⁴¹ A.J. Bray, Advances in Physics **43**, 357 (1994).
- ⁴² C. Chaillout, M.A. Alario-Franco, J.J. Capponi, J. Chenavas, J.L. Hodeau and M. Marezio, Phys. Rev. B **36**, 7118 (1987).
- ⁴³ Th. Zeiske, D. Hohlwein, R. Sonntag, F. Kubanek and G. Collin, Z. Phys. B **86**, 11 (1992).
- ⁴⁴ M. Käll, M. von Zimmermann, N.H. Andersen, J. Madsen, T. Frello, O. Schmidt, H.F. Poulsen, J.R. Schneider and Th. Wolf, unpublished.
- ⁴⁵ E. Brecht, W.W. Schmahl, H. Fuess, H. Casalta, P. Schleger, B. Lebech, N.H. Andersen and Th. Wolf, Phys. Rev. B **52**, 9601 (1995).
- ⁴⁶ T. Frello, M. Baziljevich, T.H. Johansen, N.H. Andersen and Th. Wolf, Phys. Rev. B **59**, R6639 (1999).
- ⁴⁷ D. de Fontaine, G. Ceder and M. Asta, Nature **343**, 544 (1990).
- ⁴⁸ T. Fiig, N.H. Andersen, P.-A. Lindgård, J. Berlin and O.G. Mouritsen, Phys. Rev. B **54**, 556 (1996).
- ⁴⁹ D. de Fontaine, L.T. Wille and S.C. Moss, Phys. Rev. B **36**, 5709 (1987).
- ⁵⁰ P.A. Sterne and L.T. Wille, Physica C **162-164**, 223 (1989).
- ⁵¹ A.G. Khachatryan and J.W. Morris, Phys. Rev. Lett. **64**, 1989 (1990).
- ⁵² A. Bertinotti, J. Hamann, D. Luzet and A. Vinzent, Physica C **160**, 227 (1989).
- ⁵³ F. Yakhov, V. Plakhty, A. Stratilatov, P. Burlet, J.P. Lauriat, E. Elkaim, J.Y. Henry, M. Vlasov and S. Moshkin, Physica C **261**, 315 (1996).
- ⁵⁴ T. Krekels, T.S. Shi, J. Reyes-Gasga, G. van Tendeloo, J. van Landuyt and S. Amelinckx, Physica C **167**, 677 (1990).
- ⁵⁵ T. Krekels, S. Kaesche and G. van Tendeloo, Physica C **248**, 317 (1995).
- ⁵⁶ D.J. Werder, C.H. Chen and G.P. Espinosa, Physica C **173**, 285 (1991).
- ⁵⁷ R.J. Cava, A.W. Hewat, E.A. Hewat, B. Batlogg, M.

- Marezio, K.M. Rabe, J.J. Krajewski, W.F. Peck Jr. and L.W. Rupp Jr., *Physica C* **165**, 419 (1990).
- ⁵⁸ H. Tolentino, F. Baudelet, A. Fontaine, T. Gourieux, G. Krill, J.Y. Henry and J. Rossat-Mignod, *Physica C* **192**, 115 (1992).
- ⁵⁹ H. Lüetgemeier, S. Schmenn, P. Meuffels, O. Storz, R. Schölnhorn, Ch. Niedermeier, I. Heinmaa and Yu. Baikov, *Physica C* **267**, 191 (1996).
- ⁶⁰ H.F. Poulsen, N.H. Andersen, J.V. Andersen, H. Bohr and O.G. Mouritsen, *Nature* **349**, 594 (1991).
- ⁶¹ H.F. Poulsen, N.H. Andersen, J.V. Andersen, H. Bohr and O.G. Mouritsen, *Phys. Rev. Lett.* **66**, 465 (1991).
- ⁶² J. Zaanen, A.T. Paxton, O. Jepsen and O.K. Andersen, *Phys Rev. Lett.* **60**, 2685 (1988).
- ⁶³ R. McCormack, D. de Fontaine and G. Ceder, *Phys. Rev. B* **45**, 12976 (1992).
- ⁶⁴ G. Uimin, *Phys. Rev. B* **50**, 9531 (1994).
- ⁶⁵ A.A. Aligia and J. Garcés, *Phys. Rev. B* **49**, 524 (1994).
- ⁶⁶ H. Haugerud, G. Uimin and W. Selke, *Physica C* **275**, 93 (1997).
- ⁶⁷ A.A. Aligia, J. Garcés and H. Bonadeo, *Phys. Rev. B* **42**, 10226 (1990).
- ⁶⁸ S. Semenovska and A.G. Khachaturian, *Phys. Rev. B* **46**, 6511 (1992).
- ⁶⁹ A.G. Khachaturian and J.W. Morris Jr., *Phys. Rev. Lett.* **61**, 215 (1988).
- ⁷⁰ P.A. Lindgård, N.H. Andersen, D. Mønster and T. Fiig, In: *Scientific Computing Report 1995-1997*, J. Wasniewski (Ed.), (UNI-C, Copenhagen, 1998), 38 (1998).
- ⁷¹ A.A. Aligia, J. Garcés and J.P. Abriata, *Physica C* **221**, 109 (1994).

FIG. 1. $(2.5\ 0\ 0)$ superstructure reflection of the ortho-II phase at room temperature scanned along h (left), k (middle) and l (right) in crystal #1. The thermal treatment of the crystal corresponds to state 2 as described in the text. The lines are least square fits to equation (1). The peak at $h = 2.68$ is an Al $(2\ 2\ 0)$ powder-line.

FIG. 2. Half width half maximum (HWHM) of the ortho-II superlattice peak along h , k and l plotted as function of sample mosaicity in the ac -plane of four differently grown crystals. The growth techniques are described in the text.

FIG. 3. Peak to background ratio of the ortho-II superlattice reflection $(2.5\ 0\ 5)$ plotted as function of the peak width measured at crystal #1 with $x = 0.50$ after the different thermal treatments (labeled 1 ... 6) that are described in the text. The lines are fits to a quadratic dependence of the intensity on the width.

FIG. 4. Top: $(2.5\ 0\ 5)$ peak intensity measured by ω -scans for crystal #1 with $x = 0.50$ after annealing at $80\ ^\circ\text{C}$ for 70 days and cooling to room temperature by $1\ ^\circ\text{C}/\text{hour}$ (annealing procedure 1 in Subsection III A). Open symbols mark the data obtained during heating, closed symbols those from cooling. The inset shows the slope of the data for heating (solid line) and those for cooling (dashed line) normalized to unity. Middle: Half width half maximum of the superstructure reflection. The line is a fit to the critical behavior of a 3-dimensional Ising model. Bottom: Exponent of the Lorentzian scattering function. The exponent of the data above $95\ ^\circ\text{C}$ are fixed to $y' = 1$.

FIG. 5. Ortho-III superlattice reflections measured on a crystal with oxygen composition $x = 0.72$ at room temperature. Left: $(h\ 0\ 5)$ -scan, middle: $(8/3\ k\ 0)$ -scan and right: scan along $(7/3\ 0\ l)$ (open circles) and $(8/3\ 0\ l)$ (filled circles). The lines shown with the h - and k -scan are fits to a Lorentzian function ($y' = 1$).

FIG. 6. Ortho-III transition at the oxygen composition $x = 0.72$ where the peak intensity and the width of the $(8/3\ 0\ 5)$ -reflection were measured by h -scans. The open circles show the heating data and the filled circles the data during cooling. The line in the lower graph shows the behavior described by the 2D Ising model.

FIG. 7. Scans along h (left), k (middle) and l (right) at room temperature for a crystal prepared to $x = 0.62$. The peaks in the $(h\ 0\ 0)$ -scan at $h = 2.4$ and $h = 2.6$ result from the ortho-V phase. The scattering signal at $h = 2.5$ indicates the presence of the ortho-II phase. The weak peak at $h = 2.23$ is an Al-powder line originating from the sample holder and the bump at $h = 2.83$ is unidentified. At $h = 2.1$ and $h = 2.9$ tails of the fundamental Bragg reflections are observed. In the middle part of the figure white circles show a scan along $(2.4\ k\ 0)$ and black squares a $(2.5\ k\ 0)$ -scan. The right hand side shows a $(2.5\ 0\ l)$ -scan. The arrows indicate the position of Al-powder lines.

FIG. 8. Temperature dependence of the mixed phase of ortho-II and ortho-V at the oxygen composition of $x = 0.62$. The top part plots the peak intensity of the ortho-II reflections (circles) and the ortho-V reflections (squares). Open and gray shaded symbols mark the data obtained during heating, the black filled symbols the cooling data. The bottom part of the figure shows the half width at half maximum (HWHM) of the reflections of the two phases along h .

FIG. 9. Scan along $(h\ 0\ 0)$ (left), $(2.63\ k\ 0)$ (middle) and $(2.63\ 0\ l)$ (right) in a crystal with oxygen concentration of $x=0.67$ at room temperature. The h -scan on the left hand side shows peaks at approximately $h = 2\frac{3}{8}$ and $h = 2\frac{5}{8}$ indicating the ortho-VIII phase. The peak at 2.23 is an Al-powder line. Lines shown together with the h - and k -scans are Lorentzian fits. The variation of the diffracted intensity along l is only weakly q -dependent and similar to that of the ortho-III phase.

FIG. 10. Temperature dependence of the ortho-VIII phase at $x = 0.67$ measured by h -scans on the $(2\frac{3}{8}\ 0\ 3)$ superstructure reflection. The top figure shows the peak intensity, the middle part the half width half maximum together with a fit to a critical behavior according to equation 2 with $\nu = 0.79(3)$ and the bottom the peak position. The shift in the peak position indicates a transformation from ortho-VIII to ortho-V structure between 50°C and 70°C . At 150°C the peak position corresponds to the ortho-III structure.

FIG. 11. The structural phase diagram of YBCO. The structural phases and their transition temperatures are labeled: teragonal (T), ortho-I (OI, \square), ortho-II (OII, \bullet), ortho-III (OIII, \circ), ortho-V (OV, \triangle) and ortho-VIII (OVIII, \diamond). Solid lines are guides to the eye. The dashed lines are predictions from the ASYNNNI model. The data for the T-OI transition (\square) are from Andersen *et al.*¹. The T_{OII} transition temperatures for $x = 0.35$ and $x = 0.36$ are from Poulsen *et al.*¹⁹, the upper data set for $x=0.50$ is from Schleger *et al.*⁸, and the T_{OIII} transition temperature at $x=0.77$ is from Schleger *et al.*²⁶.

FIG. 12. Top: Half width half maximum for the indicated structures as function of oxygen content. Bottom: peak to background ratio. All lines are guides to the eye.

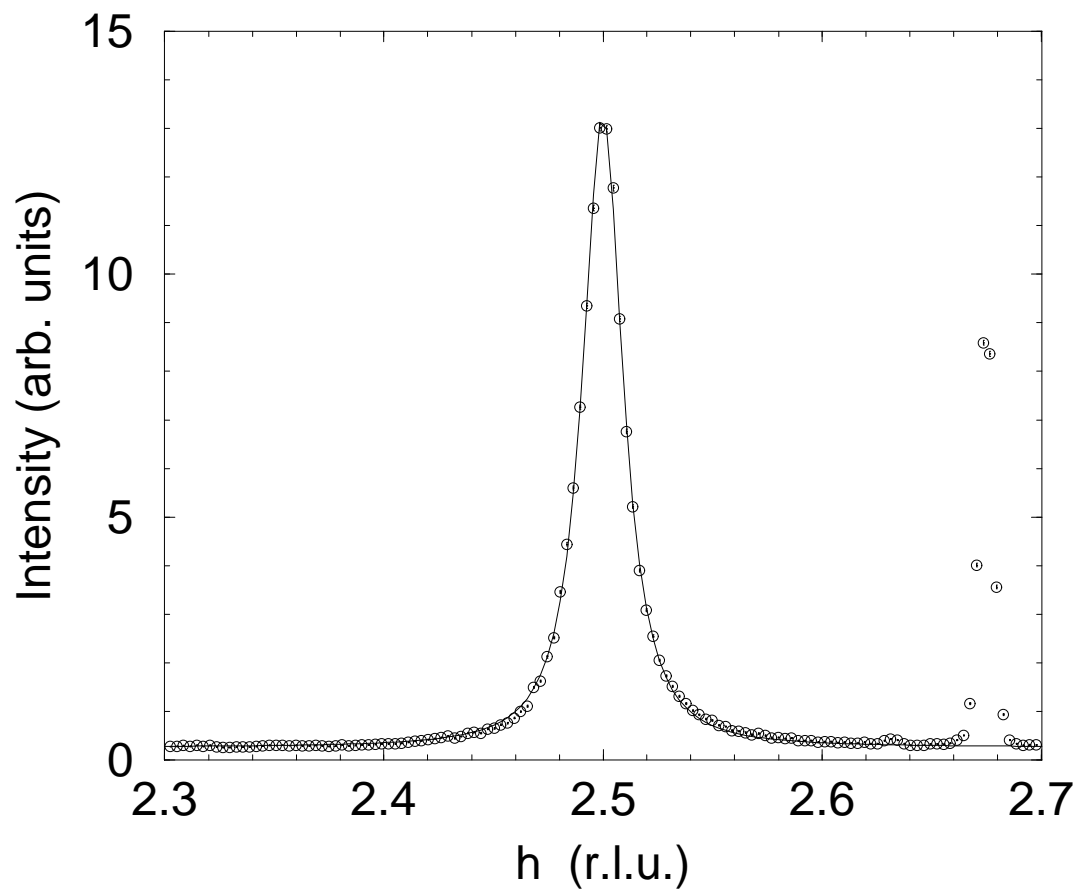


fig. 1 left

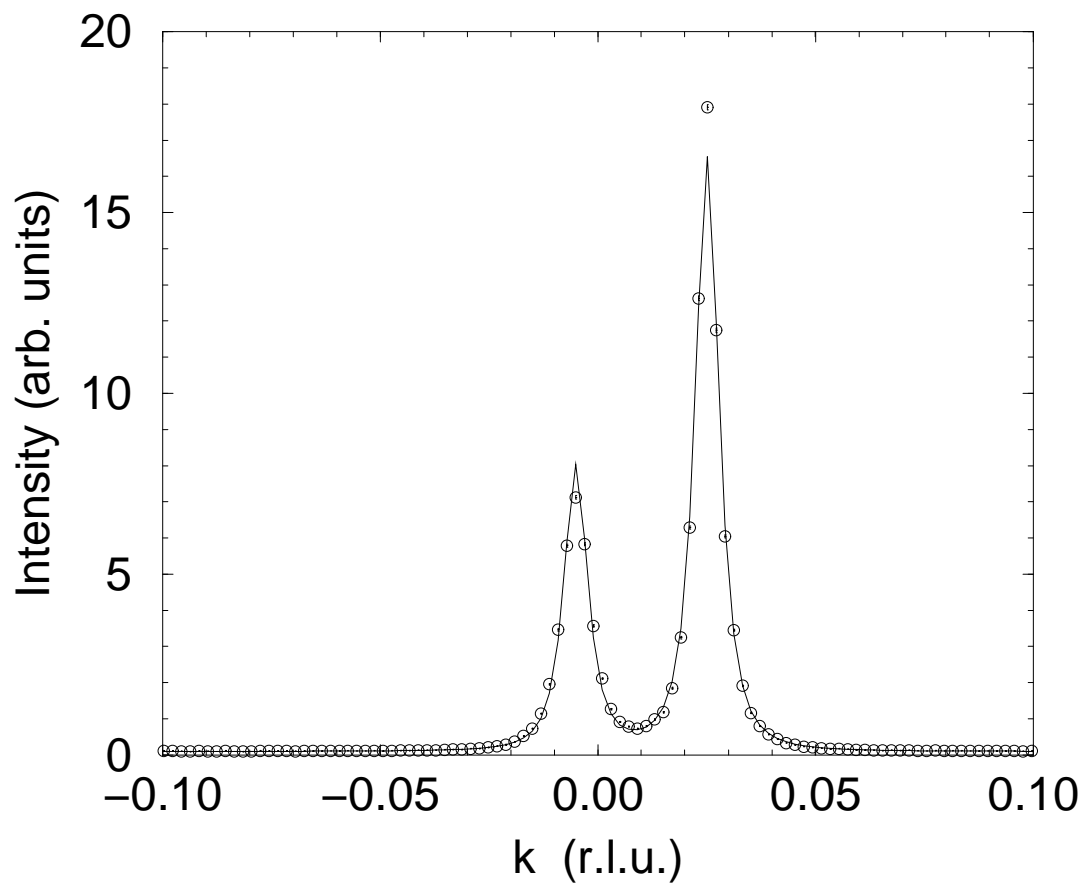


fig. 1 middle

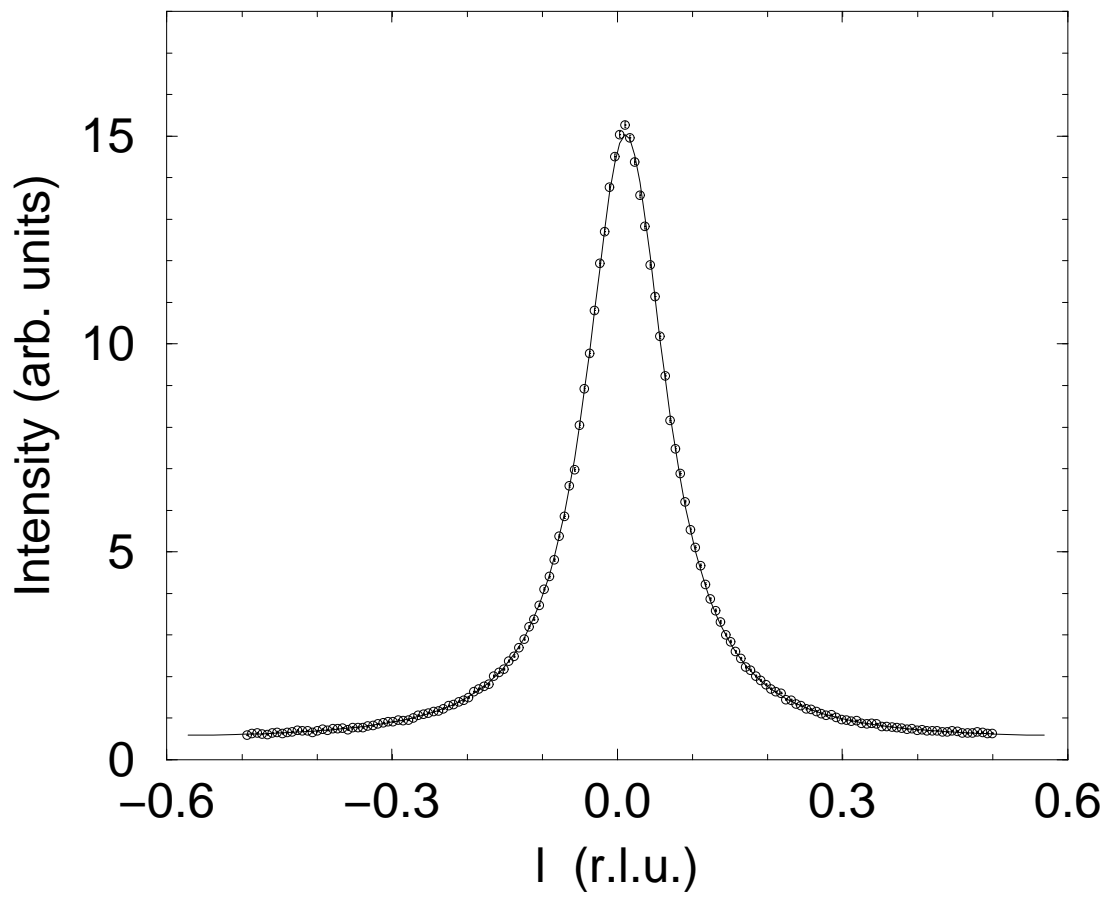


fig. 1 right

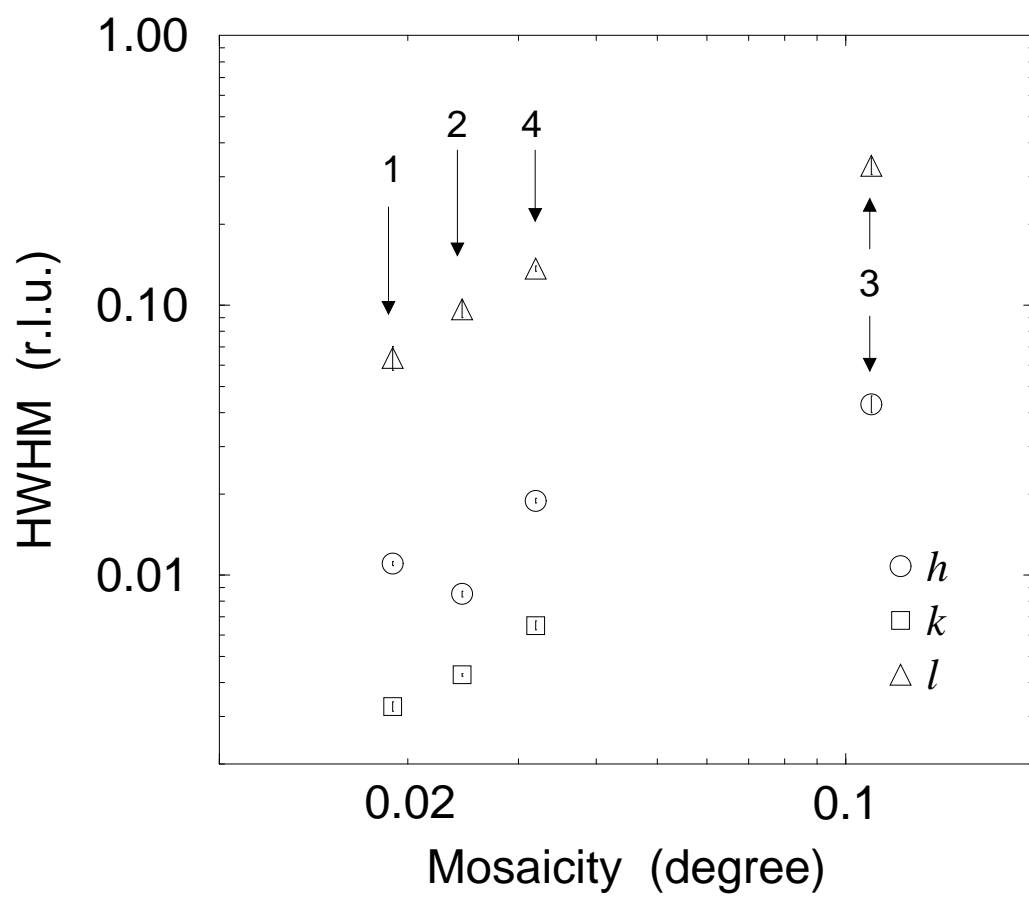


fig. 2

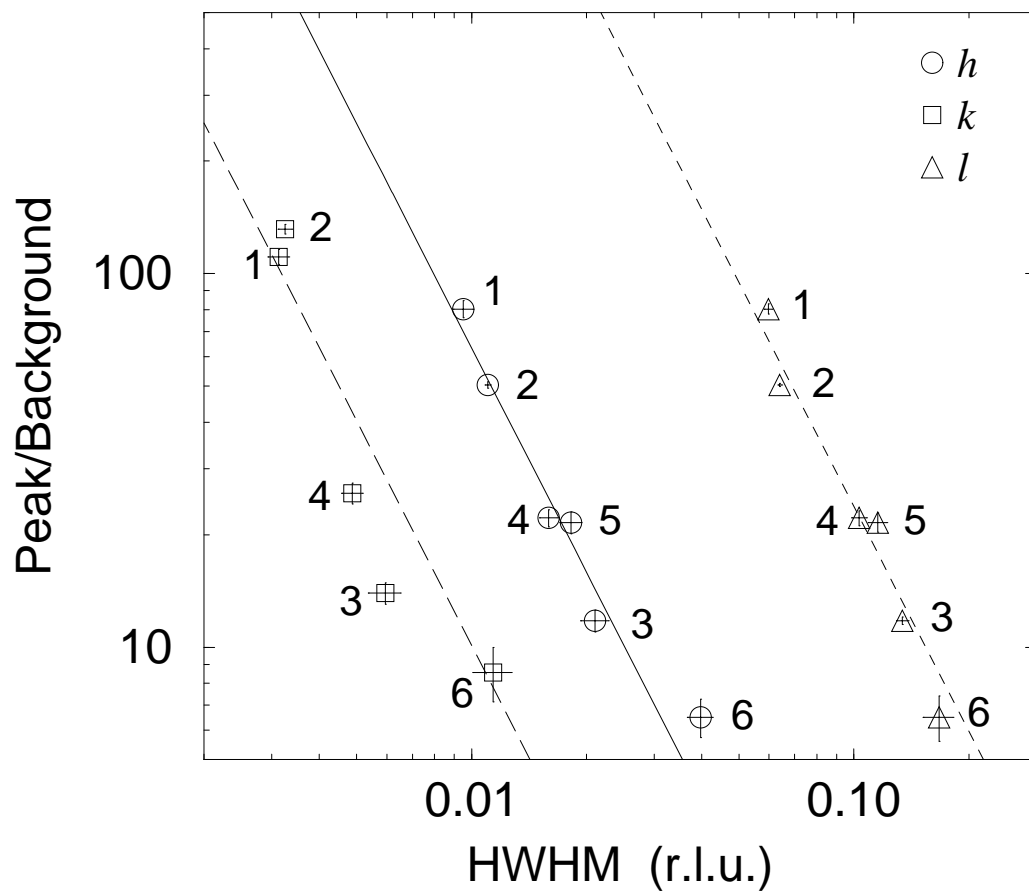


fig. 3

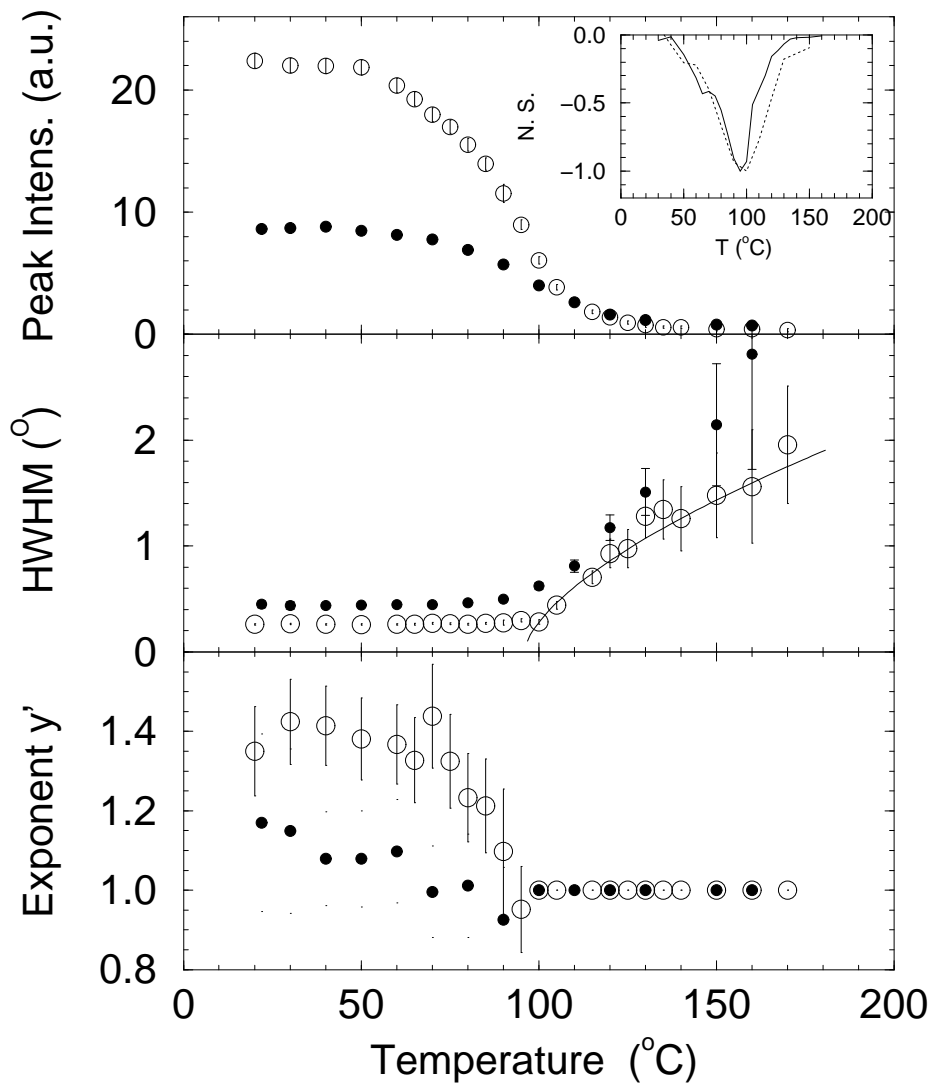


fig. 4

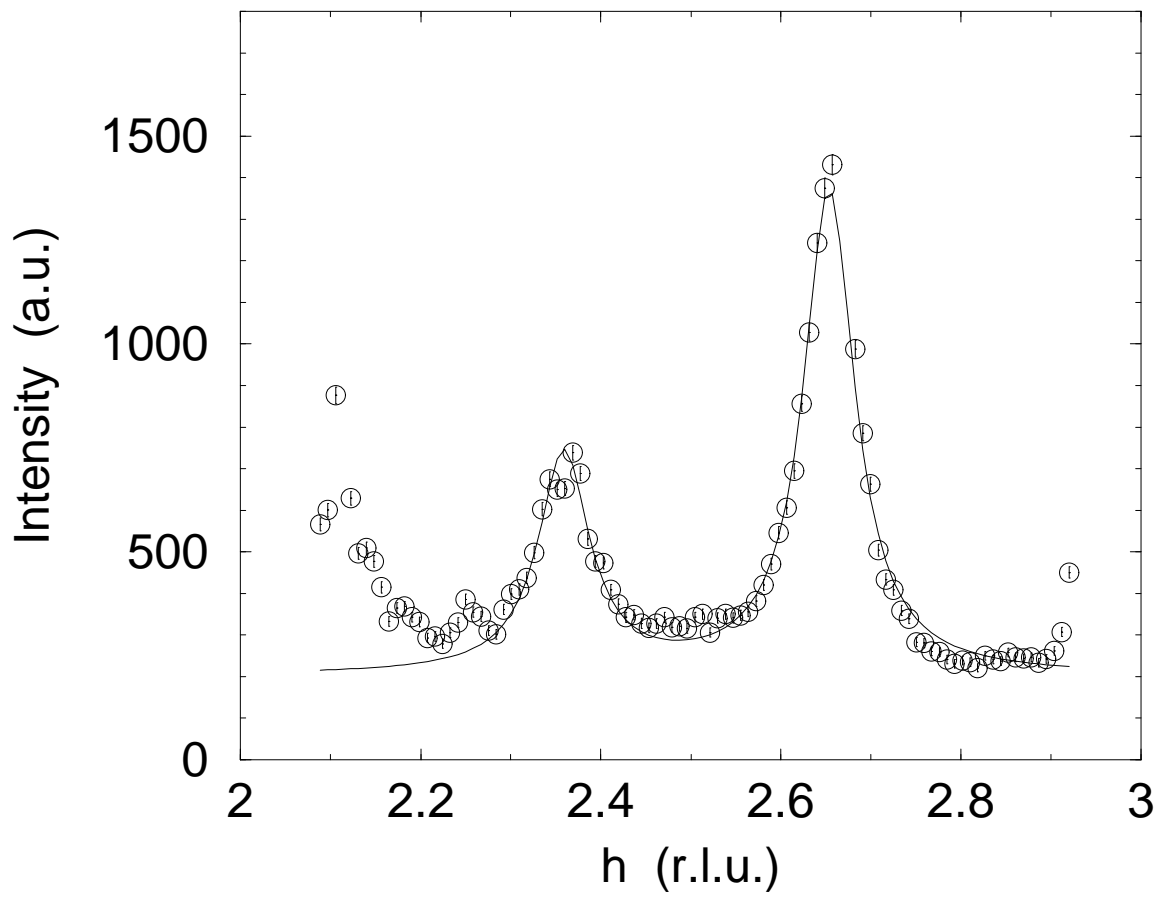


fig. 5 left

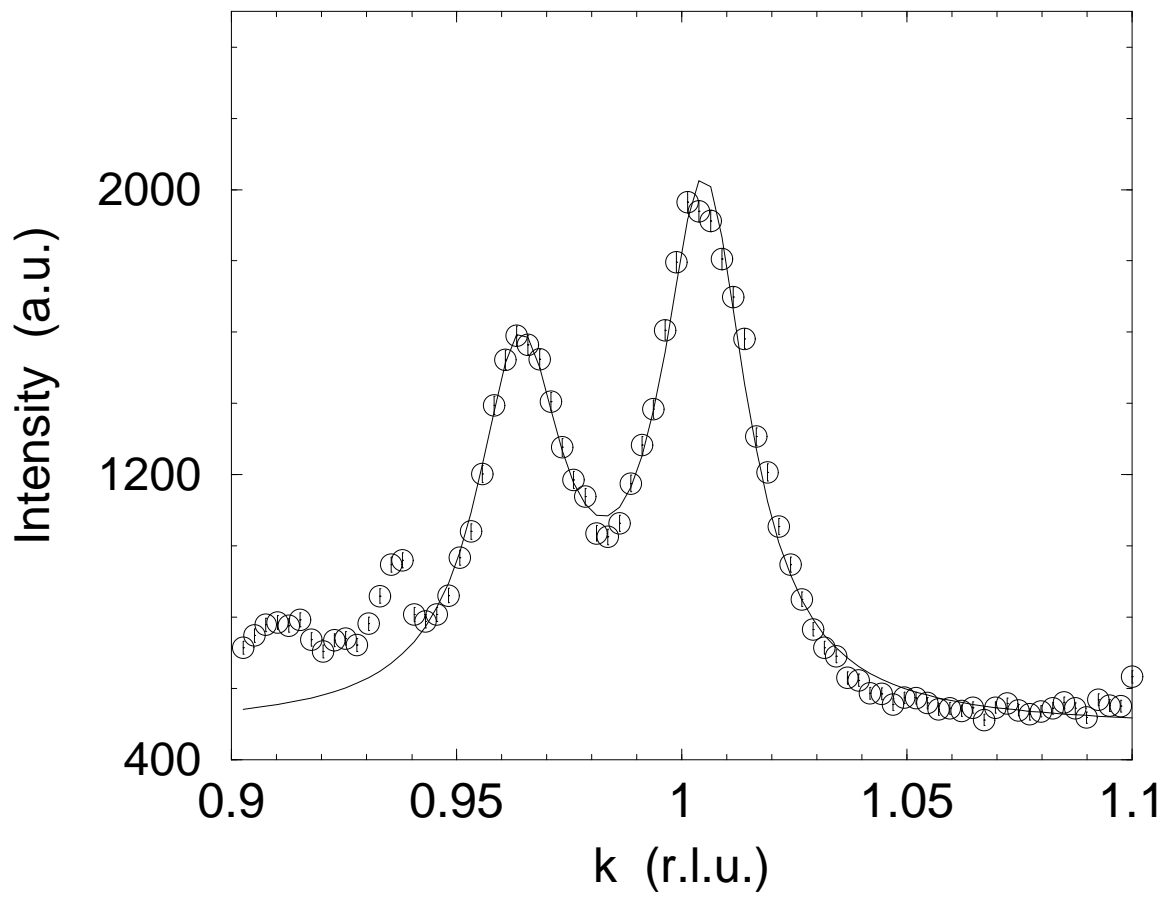


fig. 5 middle

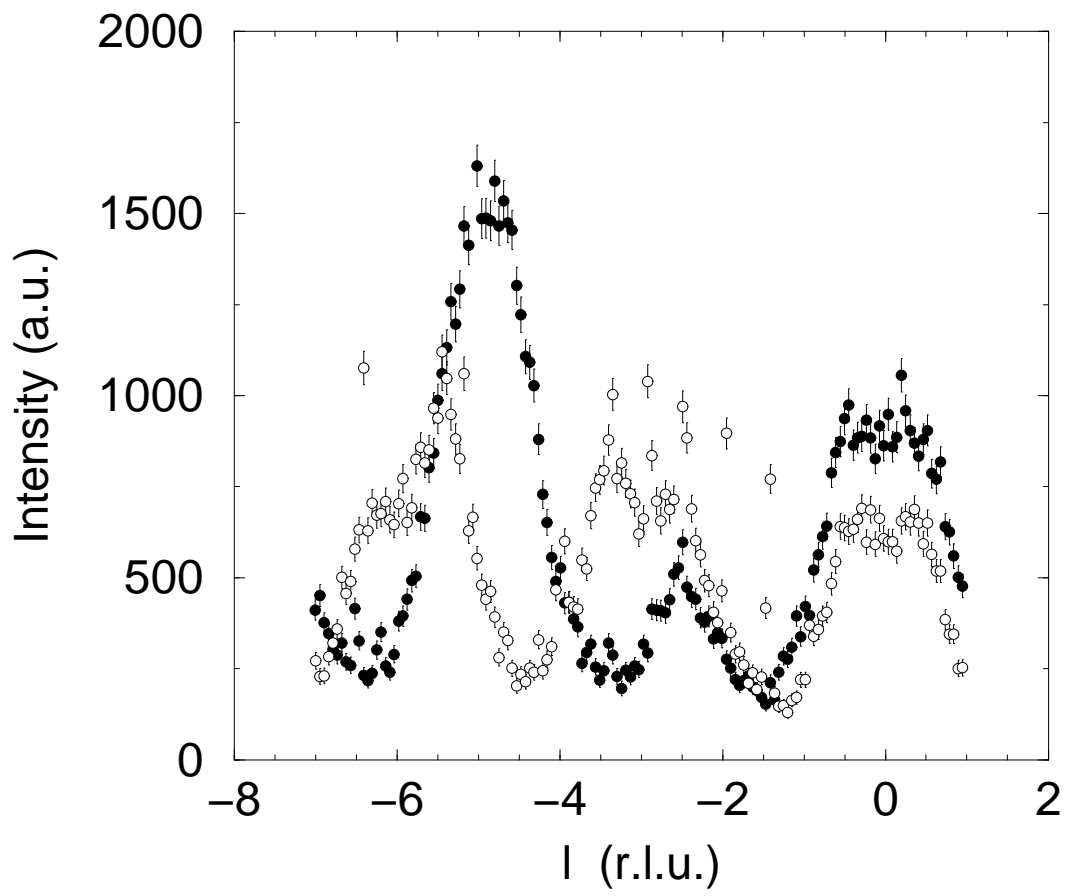


fig. 5 right

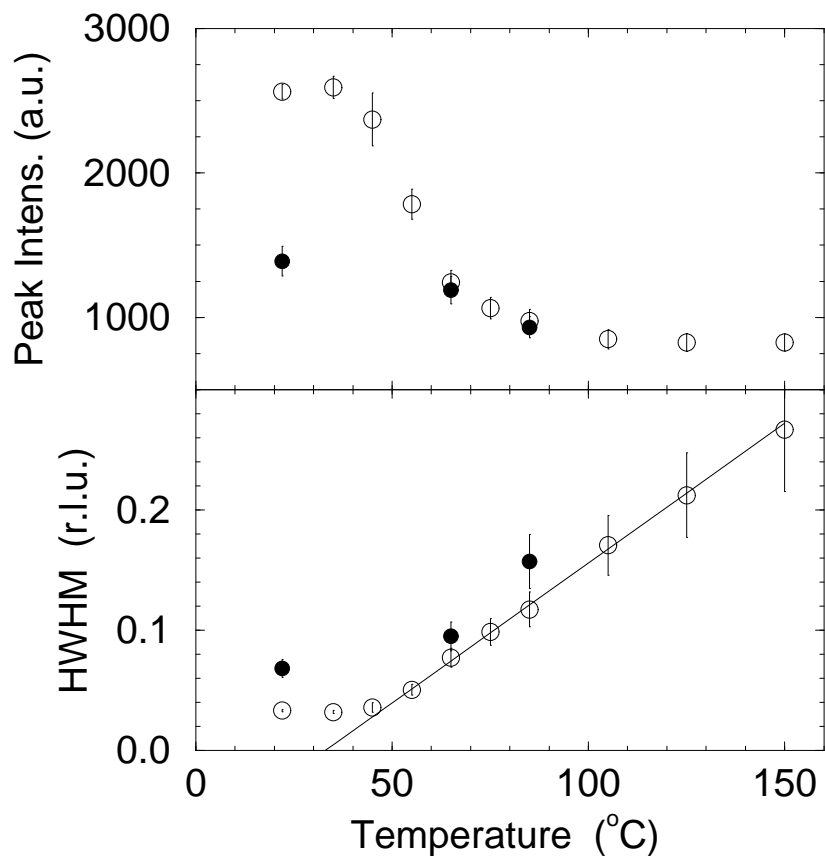


fig. 6

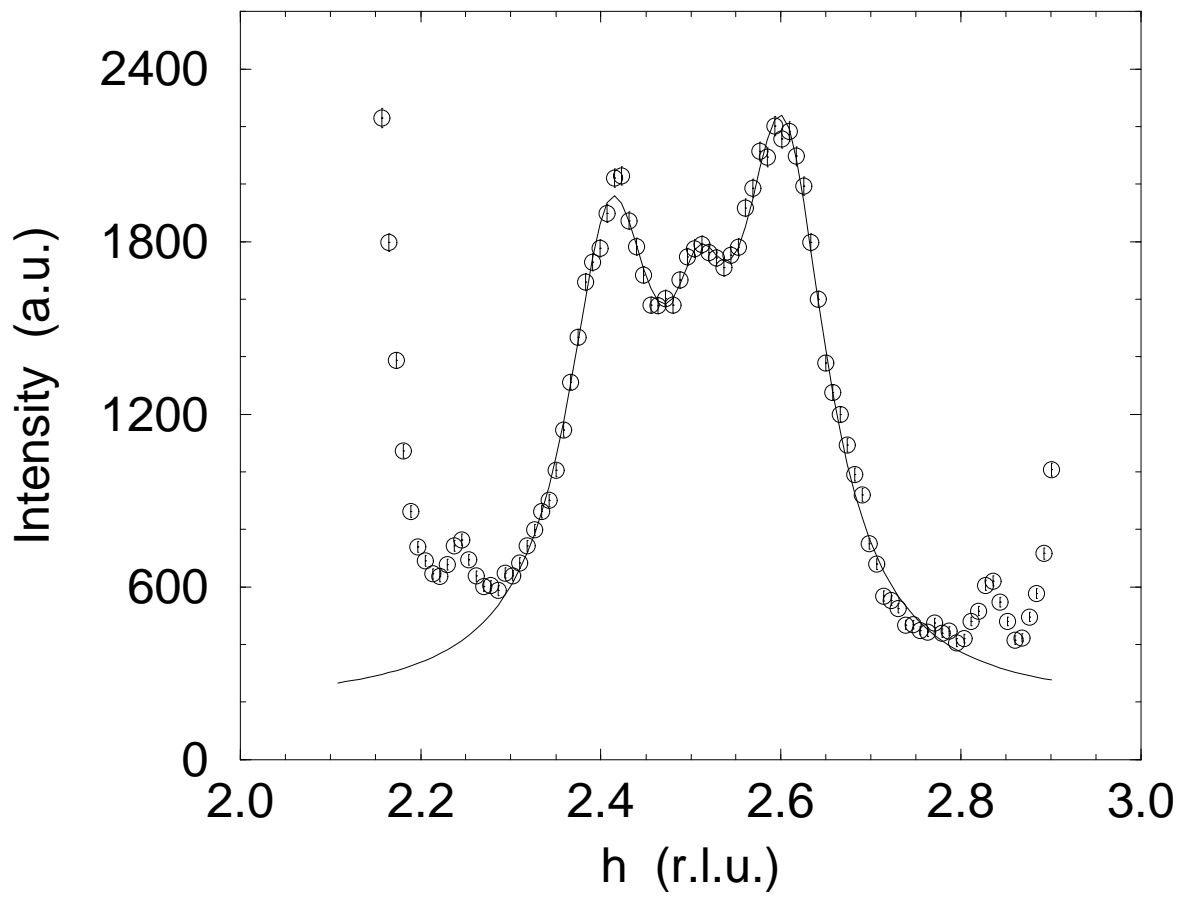


fig. 7 left

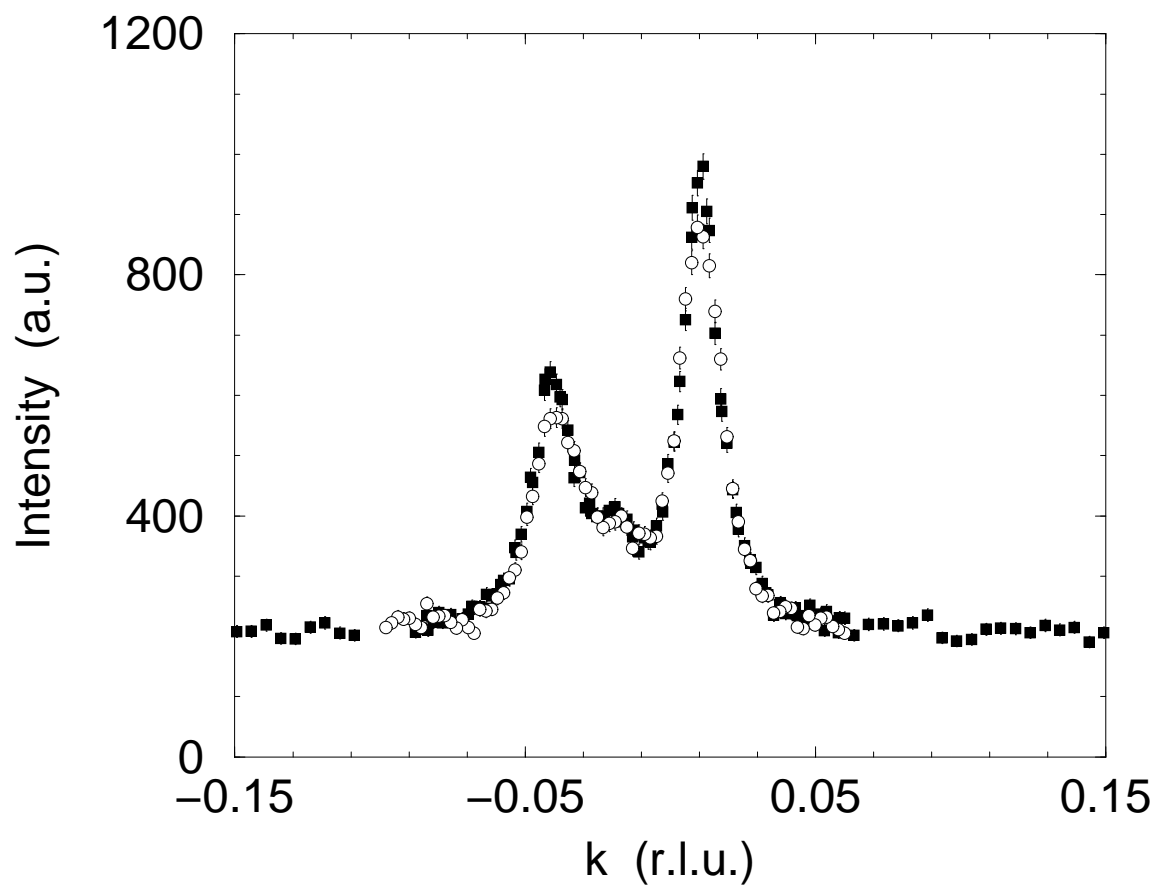


fig. 7 middle

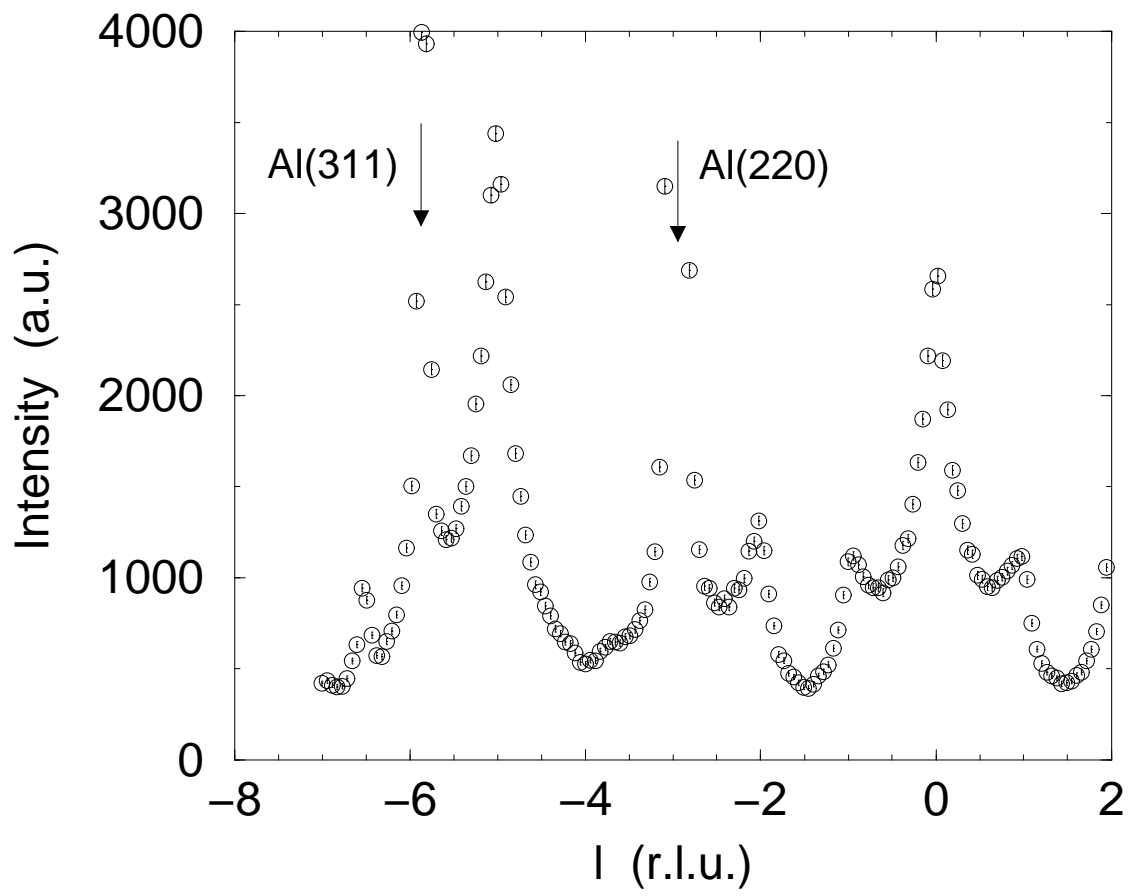


fig. 7 right

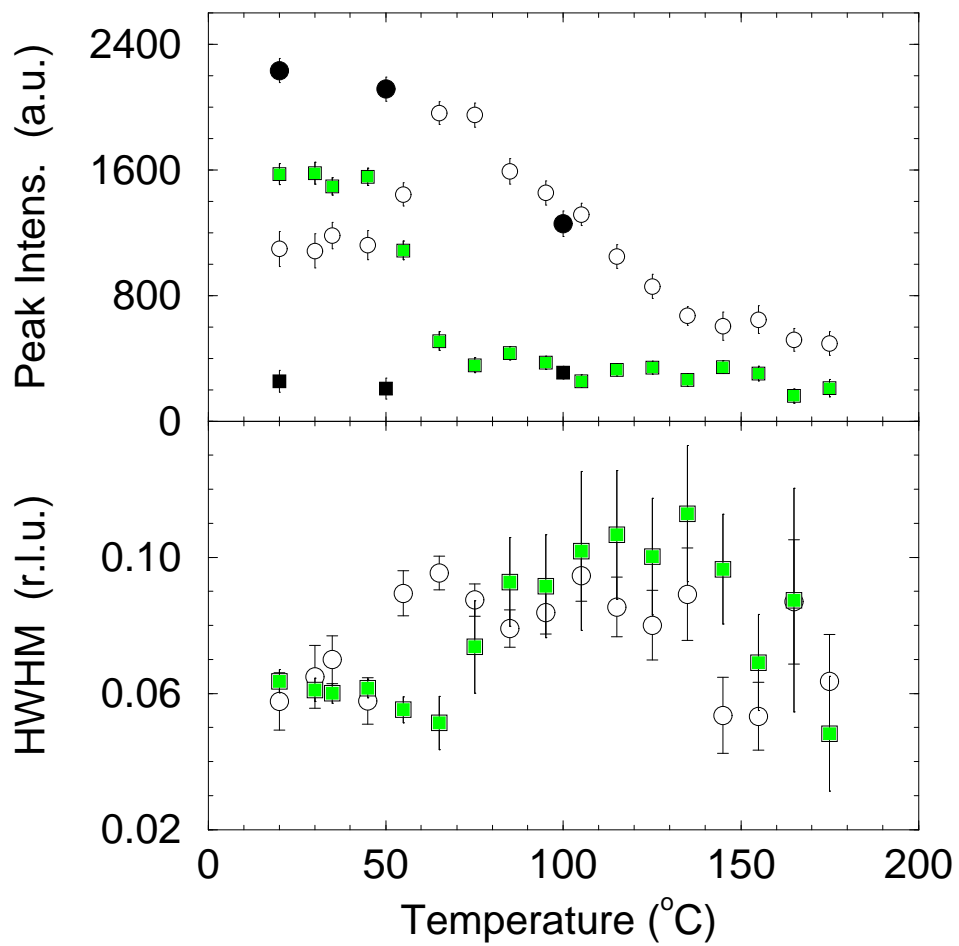


fig. 8

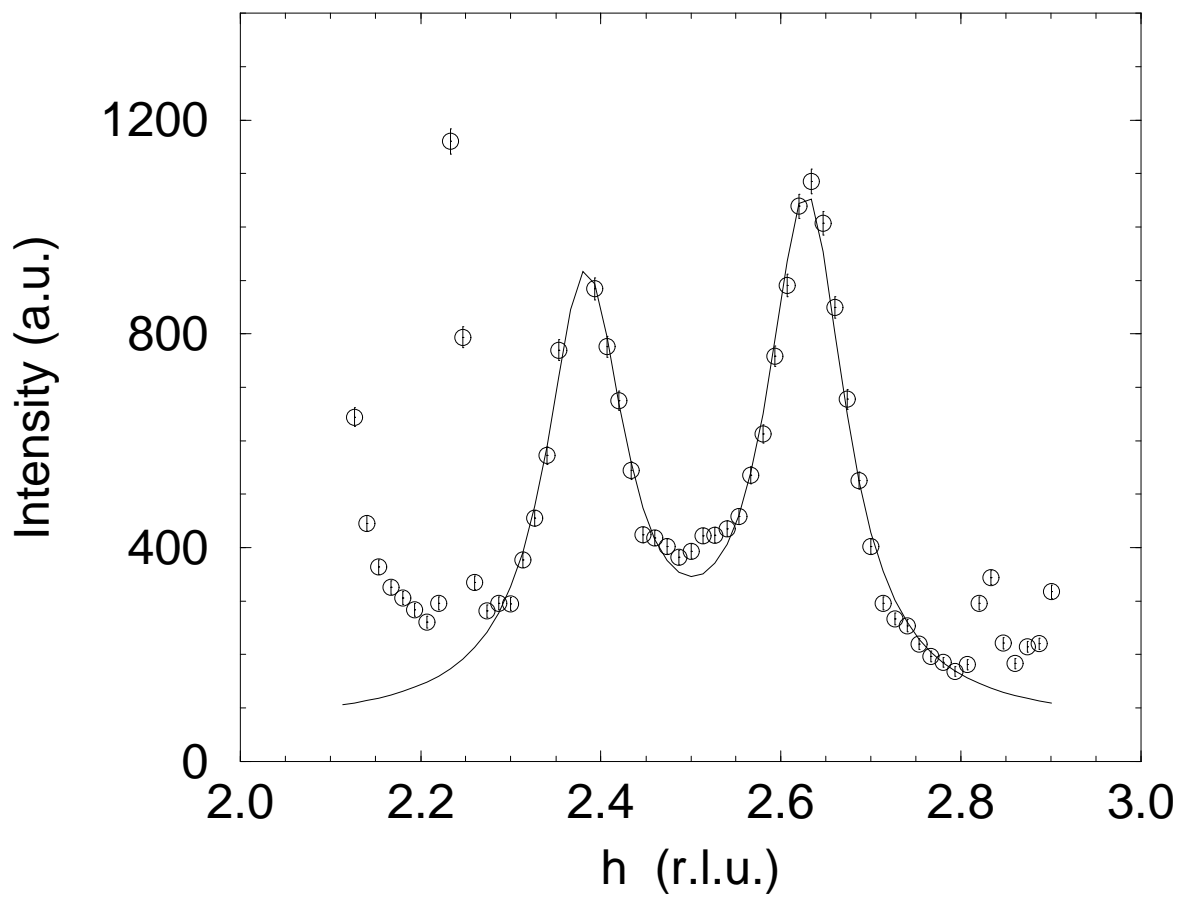


fig. 9 left

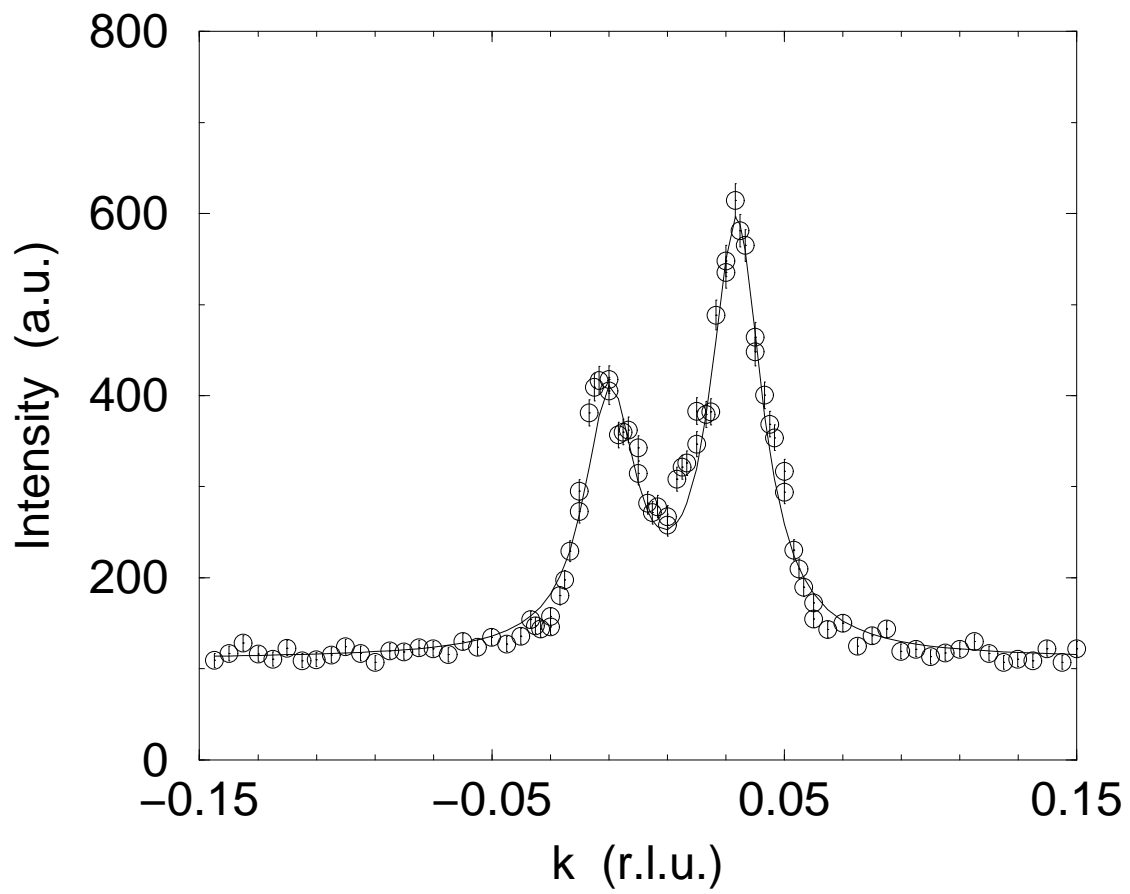


fig. 9 middle

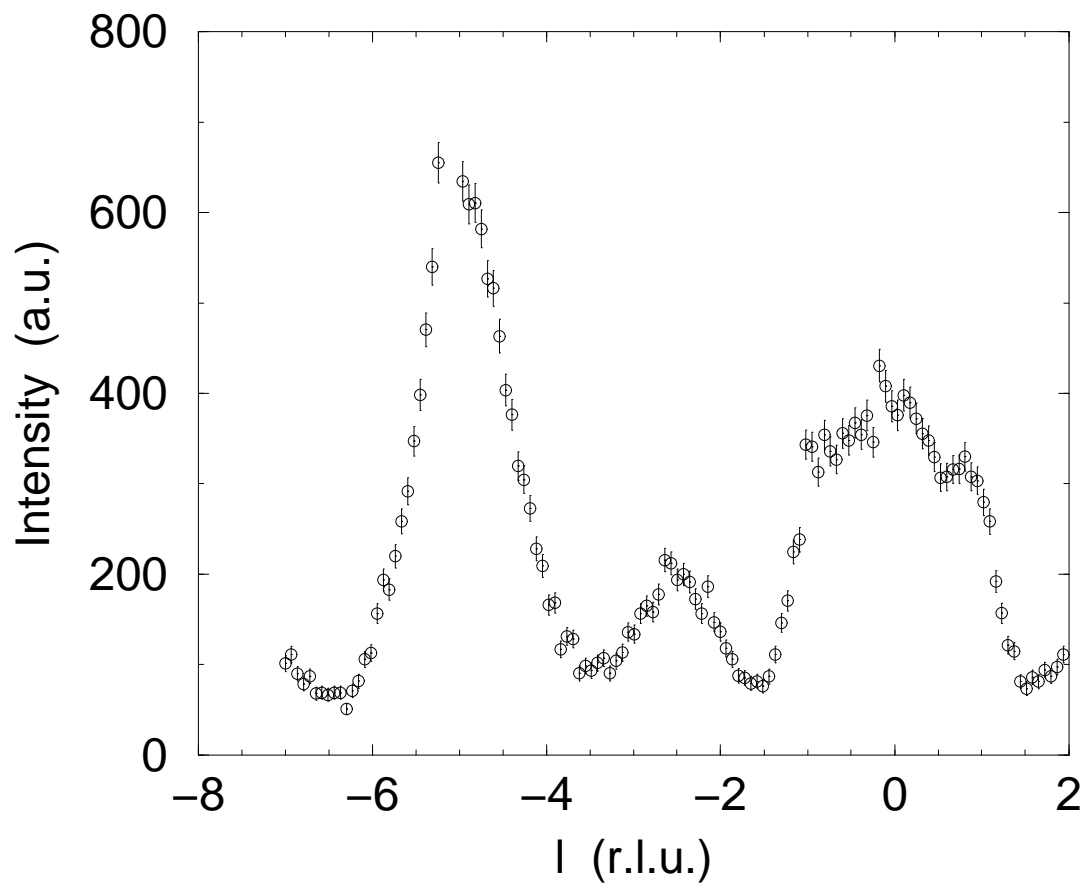


fig. 9 right

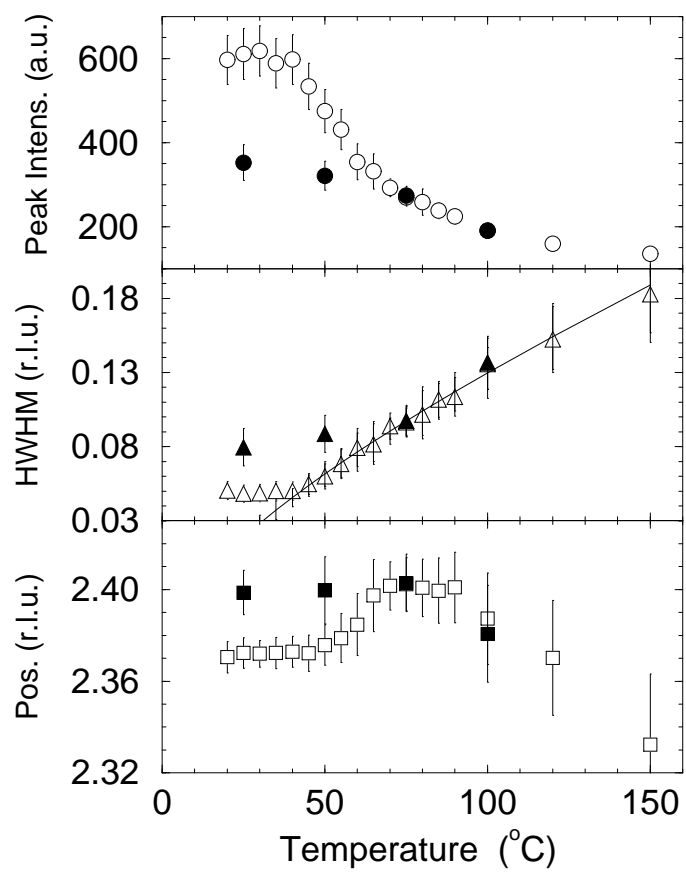


fig. 10

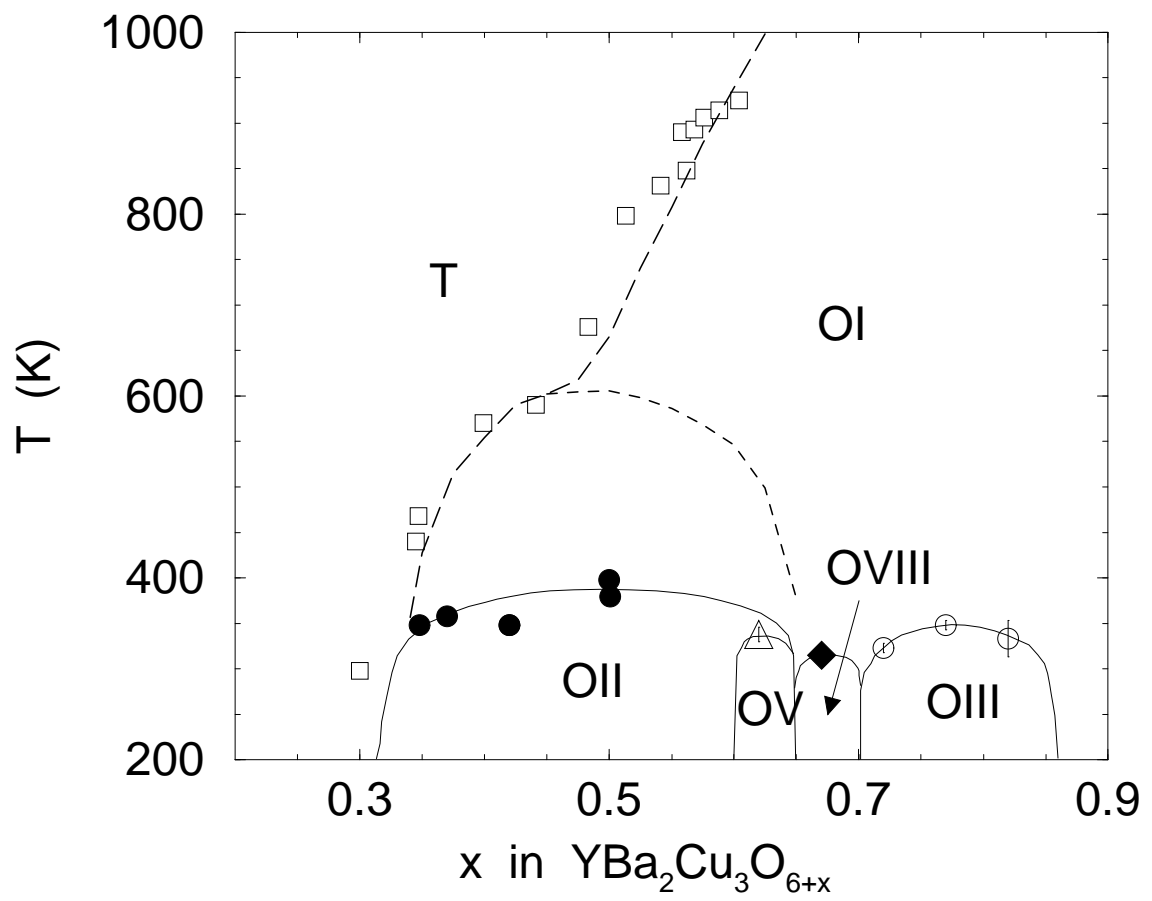


fig. 11

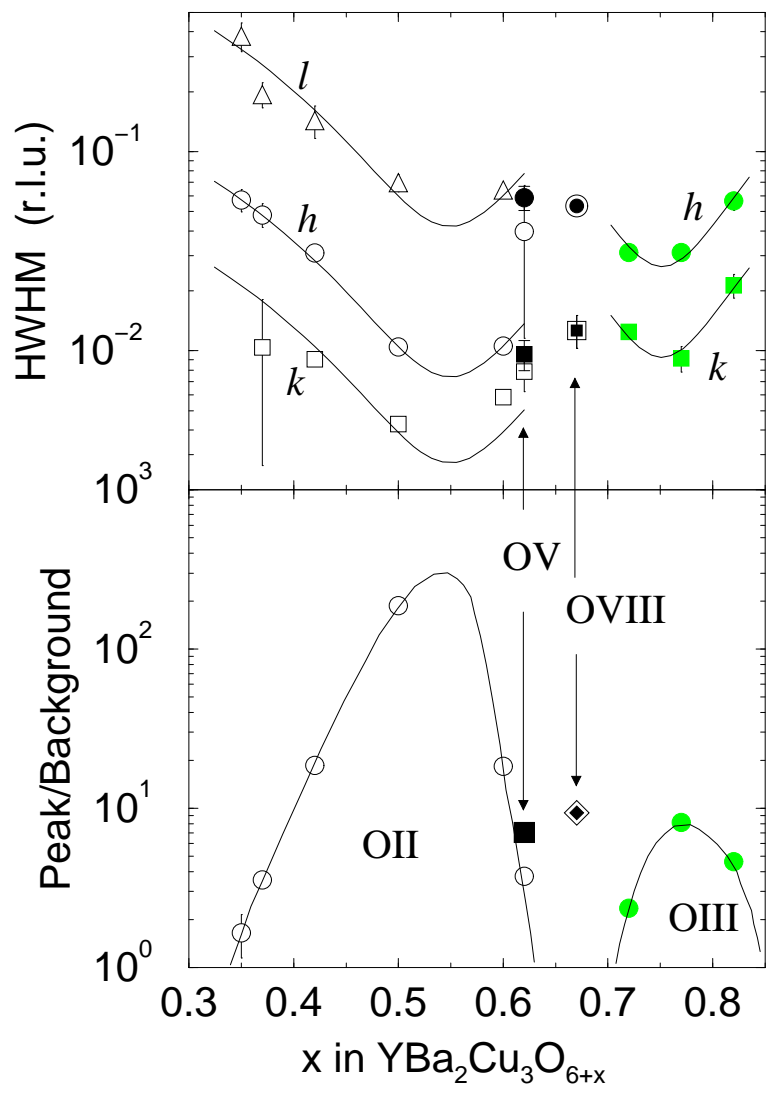


fig. 12